THE JOURNAL OF BIOLOGICAL CHEMISTRY VOL. 289, NO. 19, pp. 13419–13433, May 9, 2014

Fibulin 2, a Tyrosine *O*-Sulfated Protein, Is Up-regulated Following Retinal Detachment*

Received for publication, March 4, 2014 Published, JBC Papers in Press, April 1, 2014, DOI 10.1074/jbc.M114.562157

Yogita Kanan[1], **Daniel Brobst, Zongchao Han, Muna I. Naash, and Muayyad R. Al-Ubaidi**[2]

From the Department of Cell Biology, University of Oklahoma Health Sciences Center, Oklahoma City, Oklahoma 73104

Background: Fibulin 2 is an ECM protein of basement membranes and elastic tissues.
Results: Fibulin 2 is up-regulated during retinal detachment.
Conclusion: Up-regulation of fibulin 2 following detachment points to its role in the adhesion of the RPE to the Bruch membrane and prevention of RPE migration.
Significance: This is the first study addressing the role of fibulin 2 in retinal detachment.

Retinal detachment is the physical separation of the retina from the retinal pigment epithelium. It occurs during aging, trauma, or during a variety of retinal disorders such as age-related macular degeneration, diabetic retinopathy, retinopathy of prematurity, or as a complication following cataract surgery. This report investigates the role of fibulin 2, an extracellular component, in retinal detachment. A major mechanism for detachment resolution is enhancement of cellular adhesion between the retina and the retinal pigment epithelium and prevention of its cellular migration. This report shows that fibulin 2 is mainly present in the retinal pigment epithelium, Bruch membrane, choriocapillary, and to a lesser degree in the retina. *In vitro* studies revealed the presence of two isoforms for fibulin 2. The small isoform is located inside the cell, and the large isoform is present inside and outside the cells. Furthermore, fibulin 2 is post-translationally modified by tyrosine sulfation, and the sulfated isoform is present outside the cell, whereas the unsulfated pool is internally located. Interestingly, sulfated fibulin 2 significantly reduced the rate of cellular growth and migration. Finally, levels of fibulin 2 dramatically increased in the retinal pigment epithelium following retinal detachment, suggesting a direct role for fibulin 2 in the re-attachment of the retina to the retinal pigment epithelium. Understanding the role of fibulin 2 in enhancing retinal attachment is likely to help improve the current therapies or allow the development of new strategies for the treatment of this sight-threatening condition.

Fibulins are members of a seven-member family of extracellular matrix (ECM)[3] proteins that are important constituents of elastic fibers and basement membranes (1–5). They are divided into two classes based on their size (6). Both classes are characterized by calcium-binding EGF repeats and a C-terminal fibulin-specific module. Class I includes fibulins 1, 2, and 6, which are the larger members due to the presence of an additional N-terminal domain (absent in class II fibulins). Class II members include the shorter members fibulins 3, 4, 5, and 7 and are characterized by fewer calcium-binding EGF repeats (6).

Fibulins are known to play an essential role in cell adhesion and migration through their association with several ECM proteins and cell surface receptors such as integrins and syndecans (6, 7). Mutations in several fibulins result in human diseases (8). Mutations in fibulin 4 and fibulin 5 cause a connective tissue disorder called cutis laxa, which is characterized by cutaneous abnormalities such as loose skin (9–11). Fibulin 1 disruptions cause synpolydactyly in humans, which is characterized by malformation of distal limbs due to bone fusion (12). Fibulin 2 is down-regulated in breast cancer, colorectal cancer, lung cancer, Kaposi sarcoma, esophageal squamous cell carcinoma, nasopharyngeal carcinoma, and childhood acute lymphoblastic leukemia (13–17). The down-regulation of fibulin 2 in these cancers is either due to methylation of its promoter, gene deletion, or simply down-regulation of the levels of protein (13, 14). It was further shown in nasopharyngeal carcinoma that re-introduction of fibulin 2 expression in these tumors suppressed tumor growth in nude mice by inhibiting cell proliferation, migration, and invasion of these tumor cells (17).

Fibulin mutations have also been associated with visual defects. Mutations in fibulin 3 have been shown to cause malattia leventinese (ML), a type of inherited macular degeneration that manifests in early childhood with drusen formation in honeycomb form that makes it distinct from age-related macular degeneration (AMD) (18). Mutations in fibulins 5 and 6 were found to associate with AMD, which is characterized by drusen

* This work was supported, in whole or in part, by National Institutes of Health Grants R01EY10609 (to M. I. N.) and R01EY018137 (to M. R. A.) and Grant P30EY12190 from NEI. This work was also supported by the Oklahoma Center for the Advancement of Science and Technology (to Y. K.) and the Foundation Fighting Blindness (to M. R. A.).

[1] To whom correspondence may be addressed: Dept. of Cell Biology, University of Oklahoma Health Sciences Center, BMSB 781, 940 Stanton L. Young Blvd., Oklahoma City, OK 73104. Tel.: 405-271-2408; Fax: 405-271-3548; E-mail: ykanan@ouhsc.edu.

[2] To whom correspondence may be addressed: Dept. of Cell Biology, University of Oklahoma Health Sciences Center, BMSB 781, 940 Stanton L. Young Blvd., Oklahoma City, OK 73104. Tel.: 405-271-2382; Fax: 405-271-3548; E-mail: muayyad-al-ubaidi@ouhsc.edu.

[3] The abbreviations used are: ECM, extracellular matrix; RPE, retinal pigmented epithelium; PECS, pigmented epithelium choroid sclera; BrM, Bruchs membrane; MCL, matrix cytoplasmic lysate; TM, triple mutant; AMD, age-related macular degeneration; Fbnc, fibronectin; CC, choriocapillary; TLE, thin layer electrophoresis; ANOVA, analysis of variance; IHC, immunohistochemistry; ERD, experimental retinal detachment.

deposits beneath the retinal pigment epithelium (RPE) and central vision loss late in life (19, 20). Determination of whether mutations in fibulin 2 were associated with inherited retinal diseases led investigators to study fibulin 2 mutations in 429 controls and 402 AMD patients. Although numerous mutations were identified in the fibulin 2 gene, statistical analysis showed that these mutations were not significantly associated with AMD (19).

Fibulin 2 protein contains four major domains as follows: the N-terminal domain; three anaphylatoxin modules; 11 calcium-binding EGF repeats; and a C-terminal fibulin-type module. Its transcript has been previously identified in mouse ocular tissues (21, 22). However, little is known about the function of this protein in the eye.

In this report, we show the presence of fibulin 2 in the RPE, Bruch membrane, and choriocapillaris of ocular tissue. We provide *in vitro* and *in vivo* evidence showing that fibulin 2 is post-translationally modified by sulfation at tyrosines 192, 196, and 198, and *in vitro* elimination of these sulfated tyrosines resulted in increased cellular proliferation and migration but did not influence its secretion. Most importantly, we show that fibulin 2 is up-regulated following experimental retinal detachment and adhered to and inhibited the migration of the retinal pigment epithelial cell line ARPE19 in *in vitro* adhesion and migration assays. Therefore, we conclude that the up-regulation of fibulin 2 *in vivo* during retinal detachment suggests a role for it in the tight association between the retina and the RPE that involves a combination of its adhesive and anti-migratory characteristics, thereby allowing reattachment to the retina.

EXPERIMENTAL PROCEDURES

Recombinant Clone and Antibodies—A recombinant mouse fibulin Fbln2 clone was purchased from Genecopea. This clone was a full-length clone with a C-terminal Myc tag. The anti-Fbln2 antibody was either obtained from a commercial source (catalogue no. GTX105108, 1:1000 dilution, GeneTex) or was a kind gift from Dr. Mon-Li Chu (Thomas Jefferson University, Philadelphia, PA, dilution 1:2000) (23). The anti-Myc antibody was from Cell Signaling (catalogue no. 2276S, dilution 1:1000); the anti-fibronectin antibody was purchased from Santa Cruz Biotechnology (catalogue no. 9068, 1:200 dilution); and the anti-actin-HRP antibody was from Sigma (catalogue no. A3854, 1:25,000 dilution). The anti-sulfotyrosine antibody (PSG2, dilution 1:5000) was described previously (24) and has previously been used to enrich for tyrosine-sulfated proteins in epididymal homogenates of mice and was used as recommended (25).

Cell Lines, Transfection, and Establishment of Permanent Transfectants—The cell lines used were as follows: mouse photoreceptor cell line 661W (26); human RPE cell line ARPE19 (27); and human embryonic kidney epithelial cell lines HEK293 and HEK293T (28). HEK293T cells were transiently transfected using calcium phosphate transfection methods (29, 30). Permanent transfectants were generated by transfection into HEK293 cells and selection with 1 mg/ml geneticin (Invitrogen).

Human Donor Eyes—Human donor eyes from a normal 72-year-old Caucasian male were obtained from Lions Eye Institute (Tampa, FL) and were dissected to obtain the retina, RPE, sclera containing choriocapillaries (sclera/CC), and optic nerve tissues. Lysates were prepared from these tissues as described previously (31).

Mouse Eyes—Mouse eyes were dissected at postnatal day 25 into retina, RPE, and choroid and sclera (PECS) fractions, and lysates were prepared from these tissues as described previously (31).

Immunoblotting and Immunoprecipitation—Protein extracts were prepared from mouse and human ocular tissues, 661W cells, ARPE19 cells, and from either transiently transfected HEK293T or permanently transfected 293 cells. Protein was estimated, fractionated, and transferred to membranes and immunoblotted as described previously (31).

For the matrix cytoplasmic lysate (MCL) fractions, cells were scraped from the plates, and lysates, which contained both the matrix and cytoplasmic fractions according to previously published protocols (32), were prepared.

For the trypsin-treated MCL fractions, media were removed; cells were washed with phosphate-buffered saline (PBS) and trypsinized, following which the cells were scraped from the plates, and lysates were prepared as described above. For immunoprecipitation, 500 μg of protein extracts were incubated with the desired antibody for 12 h, precipitated by centrifugation, eluted in 1× Laemmli buffer (33), and fractionated by SDS-PAGE as described previously (31).

Fractionation of 661W cells were done according to previously published protocols (32). Briefly, 661W cells were grown to confluence in regular media and then switched to serum-free media. Media were harvested, and cells were successively treated with detergent and then 6 M urea. Lysates in the detergent fraction were enriched for nuclear and cytoplasmic proteins, and lysates in the urea fraction and media were enriched for ECM proteins.

Immunohistochemistry—Immunohistochemistry (IHC) was performed on frozen sections from eyes obtained from C57BL/6 mice at postnatal day P25, fixed in 4% paraformaldehyde in 0.1 M phosphate, and processed as described previously (34, 35). Sections were incubated with anti-Fbln2 (23) antibody.

Site-directed Mutagenesis—Site-directed mutagenesis was performed using QuikChange® II XL kit (Agilent Technologies) to Myc-tagged Fbln2 clone (WT) to create single (Y192F, Y196F, and Y198F) and triple mutants (TM) as per the manufacturer's recommendations.

Metabolic Labeling, Barium Hydroxide Hydrolysis, and Thin Layer Electrophoresis (TLE) Analysis—HEK293T cells were transiently transfected with WT, single, and TM Fbln2 clones. Eight hours after transfection, labeling media containing sulfate-free Joklik-modified Eagle's media (Sigma) containing 2% dialyzed fetal bovine serum and 0.15 mCi/ml of Na_2SO_4 (PerkinElmer Life Sciences) were added. Forty eight hours later, media were collected. Fbln2 was then immunoprecipitated from the media and fractionated by SDS-PAGE. Following transfer onto a PVDF membrane and autoradiography, the radioactive bands corresponding to Fbln2 were cut out and subjected to barium hydroxide hydrolysis and TLE analysis according to previously published methods (25, 37).

Retinal Detachment in Mice—Experimental retinal detachment was induced in P60 C57BL/6 mice via subretinal injections of 1 μl of saline as described previously by Nour *et al.* (38).

Experimental design included subretinal injection of five animals, whereas two animals served as uninjected age-matched controls. Sham injections involved inserting a needle through the sclera but not penetrating the subretinal space. The experiment was done three independent times. Protein expression on immunoblots was quantitated using the Kodak molecular imaging software version 4 (Kodak Molecular Imaging Systems). Measurements included those of background intensity, gaussian fitting the identified bands, and measurement of net intensity of each band. Finally, the net intensity values obtained for Fbln2 protein on immunoblots were divided by the values for actin to get the "levels of Fbln2."

Deglycosylation of Myc-tagged Fbln2—HEK293T cells were transiently transfected with WT and TM Fbln2 clones. Eight hours after transfection, labeling media containing sulfate-free Joklik-modified Eagle's media (Sigma) containing 2% dialyzed fetal bovine serum and 0.15 mCi/ml Na_2SO_4 (PerkinElmer Life Sciences) were added. Forty eight hours later, media were collected, and WT and TM Fbln2 clones were immunoprecipitated from the media and subjected to deglycosylation overnight at 37 °C, using the protein deglycosylation mix (New England Biolabs). The samples were then electrophoresed, followed by autoradiography and immunoblotting with anti-Myc antibody. Proteins were quantitated using Kodak Molecular Imaging software version 4, and net intensity was calculated for each sample. Bands corresponding to WT and TM Fbln2 were excised and counted for radioactivity. Finally, Fbln2 disintegration/min/Fbln2 pixels was calculated for each WT and TM Fbln2 clone.

Purification of Fbln2—Myc-tagged Fbln2 protein was affinity-purified from media of permanent transfectants using anti-Myc-agarose beads (Sigma) according to manufacturer's instructions. Media from empty vector (pcDNA3.1) permanent transfectants were passed through the affinity column and served as negative controls for the adhesion assays. The amount of purified Fbln2 eluted from the column was quantitated by SDS-PAGE alongside the known concentration of BSA standards and visualized using Coomassie Blue dye.

Adhesion Assay—For adhesion assays, 96-well plates were coated with 0.5 μg/ml BSA, Fbnc, Myc-tagged Fbln2 protein, or equivalent volumes of pcDNA3.1 vector eluent from the affinity column and allowed to air dry. The plates were then blocked with blocking buffer (3% BSA in DMEM without FBS) for 1 h at 37 °C. ARPE19 cells were dissociated and washed twice with DMEM without FBS and plated at 2×10^4 cells/well and allowed to adhere for 3 h. Nonadherent cells were washed away with PBS, and attached cells were fixed in 10% paraformaldehyde for 10 min and stained with crystal violet dye. The dye was then solubilized in 33% acetic acid, and absorbance was read at 550 nm. Absorbance values from the pcDNA3.1 vector eluent were then divided from the absorbance values of each of the purified proteins, and this value (normalized to vector) was plotted for each of the purified proteins.

Migration Assay—Migration assays were performed in 24-well CytoSelect™ cell migration assay kit containing 8-μm pore size polycarbonate membrane inserts (Cell Biolabs Inc.) according to product instructions. In migration assays comparing permanent transfectants of pcDNA 3.1 (vector), wild-type Fbln2 (WT), or the triple Tyr to Phe mutant (TM), two independent permanent transfectants of each cell type were used for the assay. The cells were pretreated with 2 μg/ml mitomycin C for 45 min, and 2×10^5 cells were plated in the upper chamber in DMEM without FBS and the lower chamber containing DMEM plus 10% FBS. Cells were incubated for 24 h at 37 °C, following which the cells that had migrated were fixed and stained with crystal violet dye, and absorbance was determined at 550 nm. The same number of cells used in the migration assay for each of the permanent transfectants was also plated and grown for 24 h in DMEM and immunoblotted with anti-actin and anti-Myc antibody.

For migration assays of ARPE19 cells, the cells were pretreated with 2 μg/ml mitomycin C for 45 min, and 1×10^5 cells were plated in the upper chamber in DMEM F-12 without FBS media and conditioned media from permanent transfectants pcDNA 3.1 (vector), or wild-type (WT) Fbln2 containing 10% FBS was added to the lower chamber. In the immunodepletion experiments, media from wild-type Fbln2 were subjected to immunoprecipitation with anti-Myc or IgG antibodies to remove Myc-tagged Fbln2 from the media. These media were then supplemented with 10% FBS and added to the lower chamber. The rest of the experiment was as described above.

Statistical Analysis—Statistical analysis was done using GraphPad Prism® software using one-way or two-way analysis of variance (ANOVA) or Student's *t* test.

RESULTS

Fibulin 2 Is Present in the Retina, RPE Bruch Membrane, and Choroid—IHC analysis on sections of P30 pigmented mouse eyes showed that Fbln2 is observed in the CC, BrM, and sclera (*green label,* Fig. 1, *A*, *C,* and *D*). Labeling, although weaker, was observed in the retina, mainly around blood vessels, as observed by the Fbln2 and endothelial marker CD31 co-staining (*arrows,* Fig. 1*A*). Equivalent amount of rabbit IgG as control showed no labeling in the eye (Fig. 1*B*). Higher ×100 magnification images showed Fbln2 labeling in BrM (*arrowheads,* Fig. 1, *C* and *D*) and choriocapillaries (Fig. 1, *C* and *D*). Also, a lumen in the choriocapillary region is visible by the staining of the endothelial marker anti-CD31 label (*Lu,* Fig. 1, *C* and *D, red*). Because the presence of pigment masks the expression of Fbln2 in the RPE of C57BL/6 eyes, immunostaining for Fbln2 was done on P30 BALB/c albino mouse eyes. Minor Fbln2 labeling is observed in the RPE (*asterisk,* Fig. 1*E*).

Further confirmation of the IHC findings came from immunoblot analysis of two independent lysates of mouse retinas and PECS. Fbln2 was mainly observed in the PECS lysates (*lanes 1* and *2*, Fig. 1*F*), whereas retinal lysates showed reduced amounts of Fbln2 (*lanes 3* and *4*, Fig. 1*F*). Interestingly, we also observed Fbln2 in conditioned media from 661W cells, a cone-specific cell line (*lane 5,* Fig. 1*F*) (26).

Because it is difficult to fractionate mouse PECS into its individual components, lysates were prepared from human donor eyes divided into optic nerve region, sclera/CC, RPE, and retina. Fig. 1*G* shows the presence of Fbln2 in the optic nerve region, sclera/CC, and RPE lysates (*lanes 1–3*), and immunoreactivity is only obvious in the retina upon prolonged exposure (data not

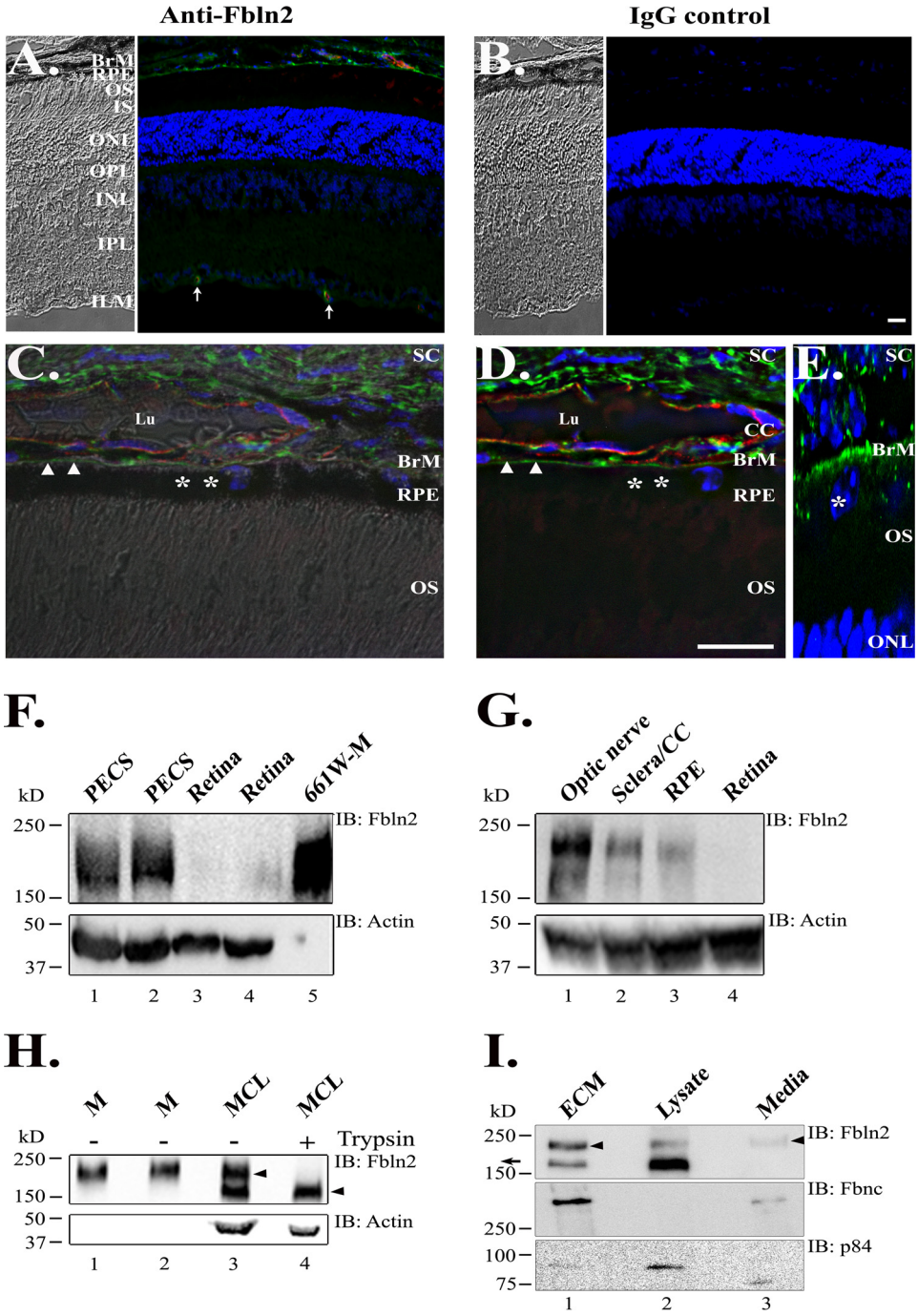

FIGURE 1. **Ocular localization of Fbln2.** Immunohistochemical labeling was performed on frozen P30-pigmented C57BL/6 mouse eye sections using anti-Fbln2 antibody (*green label*), anti-CD31 (*red label*), and rabbit IgG (*green label*) as negative control and DAP1 (*blue*). Bright field images were taken at ×20 (*A* and *B*). Mouse sections were double-stained with Fbln2 (*green*) and CD31 (*red*) and imaged at ×20 magnification (*A*). Sections stained with rabbit IgG (*green*) were imaged at ×20 magnification (*B*). Higher magnification images (×100) of sections double-stained with Fbln2 (*green*) and CD31 (*red*) superimposed on bright field images (*C*) or without the bright field are shown (*D*). *Asterisks* indicate RPE layer; *arrows* show the presence of two blood vessels in the retina; and *arrowheads* indicate Bruch membrane. All blood vessels, including choriocapillaries, are shown by the endothelial marker CD31 (*red*). A lumen of a vessel (*lu*) is shown at ×100 magnification (*C* and *D*). Higher magnification image (×100) of albino mouse eye showing sclera (*SC*), BrM, RPE (represented by an *asterisk*), outer segment (*OS*), outer nuclear layer (*ONL*), showing Fbln2 *green label* (*E*). *IPL*, inner plexiform layer; *OPL*, outer plexiform layer; *ILM*, inner limiting membrane; *INL*, inner nuclear layer *Scale bar,* 20 μm. *F,* immunoblot (*IB*) analysis of Fbln2 on conditioned media from the mouse photoreceptor cell line 661W (*lane 5*) and 50 μg of protein lysates from two independent P25 mouse eye fractions, the retina (*lanes 3* and *4*) and PECS (*lanes 1* and *2*). Samples were fractionated by 10% SDS-PAGE and transferred to PVDF membranes and immunoblotted with either anti-Fbln2 antibody or anti-actin HRP antibody. *G,* immunoblot analysis of 50 μg of protein lysates from human ocular tissue fractionated into optic nerve (*lane 1*), sclera plus choriocapillaries (*Sclera/CC*, *lane 2*), RPE (*lane 3*), and retina (*lane 4*) using anti-Fbln2 antibody. *H,* immunoblot analysis of conditioned media and matrix cytoplasmic lysates (*MCL*) from 661W cells. Media (*lane M*) were removed from two independent 661W samples before trypsin treatment (*lanes 1* and *2*), and 15 μl of the conditioned media along with 50 μg of MCL from cells untreated (*lane 3*) or treated with trypsin (*lane 4*) were immunoblotted. *I,* immunoblot analysis of Fbln2 expression in different fractions of 661W cells. Serum-free culture media (*Media*) were harvested, followed by successive extracts obtained with detergent and 6 M urea. The detergent fraction is enriched for proteins present in the nucleus and cytoplasm (*lysates*), and the urea fraction is enriched for ECM proteins (*ECM*). The blots were probed with anti-Fbln2, anti-Fbnc, and anti-p84 antibodies.

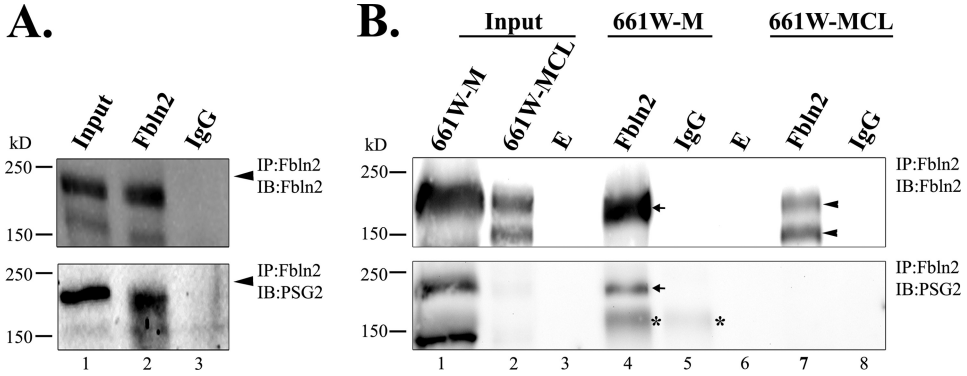

FIGURE 2. **Fbln2 is sulfated *in vivo*.** *A,* immunoprecipitation (*IP*) of Fbln2 was done from 500 μg of mouse eyecup extracts using anti-Fbln2 antibody (*lane 2*) or IgG (*lane 3*). Immunoprecipitants were electrophoresed and immunoblotted (*IB*) using anti-Fbln2 antibody or anti-sulfotyrosine antibody. *B,* Fbln2 was immunoprecipitated from 500 μl of conditioned media (*lanes 4* and *5*) and 500 μg of MCL (*lane 7* and *8*) of mouse retinal cell line 661W with anti-Fbln2 antibody (*lanes 4* and *7*) or IgG (*lanes 5* and *8*). Immunoprecipitants were immunoblotted with either anti-Fbln2 antibody or with PSG2. *Arrowheads* point to the two isoforms of Fbln2 identified. *Arrow* points to the only isoform of Fbln2 that was recognized as sulfated by PSG2. Bands marked with *asterisks* are nonspecific. *Lanes 3* and *6* are empty lanes (*E*).

shown), in agreement with observed reduced levels in the mouse retina (Fig. 1*F*).

Although very little Fbln2 was observed in retinal lysates (Fig. 1, *F* and *G*), high levels of Fbln2 were detected (*lane 5,* Fig. 1*F*) in conditioned media from 661W cells (26, 39). Fbln2 produced by 661W cells exists both in the media and in the fraction that contains both matrix and cytoplasmic proteins, herein named MCL. When the conditioned media and MCL fractions were probed with anti-Fbln2 antibody, the MCL fraction was found to harbor two isoforms of Fbln2, a 195-kDa and a 160-kDa isoform (*lane 3, arrowheads,* Fig. 1*H*), although the 195-kDa isoform was mainly detected in the media (*lanes 1* and *2*, Fig. 1*H*). To differentiate between external or matrix fractions and the internal or cytoplasmic fractions, 661W cells were subjected to brief trypsin treatment to remove ECM or matrix-attached Fbln2. As a control, another 661W sample was treated with saline. Lysates were then electrophoresed alongside conditioned media on SDS-PAGE. Interestingly, immunoblot analysis of these lysates showed that the 195-kDa Fbln2 (*upper arrowhead*) isoform was eliminated from the MCL fraction after trypsin treatment leaving the 160-kDa band (*lower arrowhead*) unaffected (compare *lanes 3* and *4*, Fig. 1*H*). However, media prior to trypsin treatment showed the presence of the 195-kDa Fbln2 band (*lanes 1* and *2,* Fig. 1*H*). Trypsin digestion of the 195-kDa isoform of Fbln2 in MCL proved that this isoform is located outside the cell, consistent with its ECM or matrix association and thereby its susceptibility to trypsin cleavage. The trypsin resistance of the shorter 160-kDa isoform suggests that this isoform is still present inside the cell and is not secreted into the ECM fraction of 661W cells.

To further separate the MCL fraction into cytoplasmic and ECM fractions and to verify the extracellular status of the 195-kDa isoform of Fbln2, 661W cells were fractionated according to a previously established method (32) wherein the 661W cells were grown to confluence in regular media and then switched to serum-free media. After removing the media, cells were treated successively with a detergent solution, followed by urea solution. It has been previously established that the detergent fraction is enriched in cytoplasmic and nuclear proteins, and the urea and media fractions are enriched in ECM proteins (32). The lysates and media were then electrophoresed alongside conditioned media on SDS-PAGE. Immunoblot analysis with an ECM-specific marker, Fbnc (32), shows that the 195-kDa Fbln2 isoform is enriched in the media (only 2% of the total media was run), and the ECM-urea fraction (*arrowheads, lanes 1* and *3*, Fig. 1*I*) is similar to Fbnc. The 160-kDa Fbln2 isoform is enriched in the cytoplasmic and nuclear fractions, similar to the nuclear matrix protein p84 (*lane 2,* Fig. 1*I*).

Fibulin 2 Is a Tyrosine-sulfated Protein—In the course of isolating retinal tyrosine-sulfated proteins by a PSG2 affinity chromatography column (24) followed by tandem mass spectrometric analysis, Fbln2 was identified (data not shown). To verify that Fbln2 is indeed tyrosine-sulfated, it was immunoprecipitated from postnatal day 1 mouse eyecup lysates. Fig. 2*A* shows the 195-kDa isoform of Fbln2 was specifically pulled down by the anti-Fbln2 antibody but not by mouse IgG (compare *lanes 2* and *3*, Fig. 2*A*, *IB:Fbln2*). This 195-kDa isoform was also identified by PSG2 to be tyrosine-sulfated (*lane 2,* Fig. 2*A*, *IB:PSG2*).

Because Fbln2 was observed in the media and MCL fractions of 661W cells (Fig. 1*H*), conditioned media and MCL were subjected to immunoprecipitation with equivalent amounts of anti-Fbln2 and IgG antibodies. Although only the 195-kDa isoform was pulled down from the conditioned media with anti-Fbln2 antibody and not IgG (*arrow,* compare *lanes 4* and *5*, Fig. 2*B*, *IB:Fbln2*), both the 195- and 160-kDa isoforms were immunoprecipitated from the MCL with anti-Fbln2 antibody and not IgG (*arrowheads,* compare *lanes 7* and *8*, Fig. 2*B*, *IB:Fbln2*). However, PSG2 only recognized the 195-kDa isoform in the media (*arrow, lane 4,* Fig. 2*B*, *IB:PSG2*) to be tyrosine-sulfated. Both isoforms from the MCL were not recognized by PSG2 (*lane 7,* Fig. 2*B*, *IB:PSG2*) to be tyrosine-sulfated. A nonspecific band that is immunoprecipitated from the conditioned media and recognized by the PSG2 antibody to be tyrosine-sulfated is marked by an *asterisk* (see *lanes 4* and *5,* Fig. 2*B*, *IB:PSG2*) and could be a component of bovine serum present in the media or secreted by the cells.

Fibulin 2 Is Also Tyrosine-sulfated in Vitro—To determine whether Fbln2 is tyrosine-sulfated *in vitro*, a recombinant wild-type Fbln2 with a C-terminal Myc tag and a control pcDNA 3.1 plasmid (vector) were transfected into HEK293T cells. Follow-

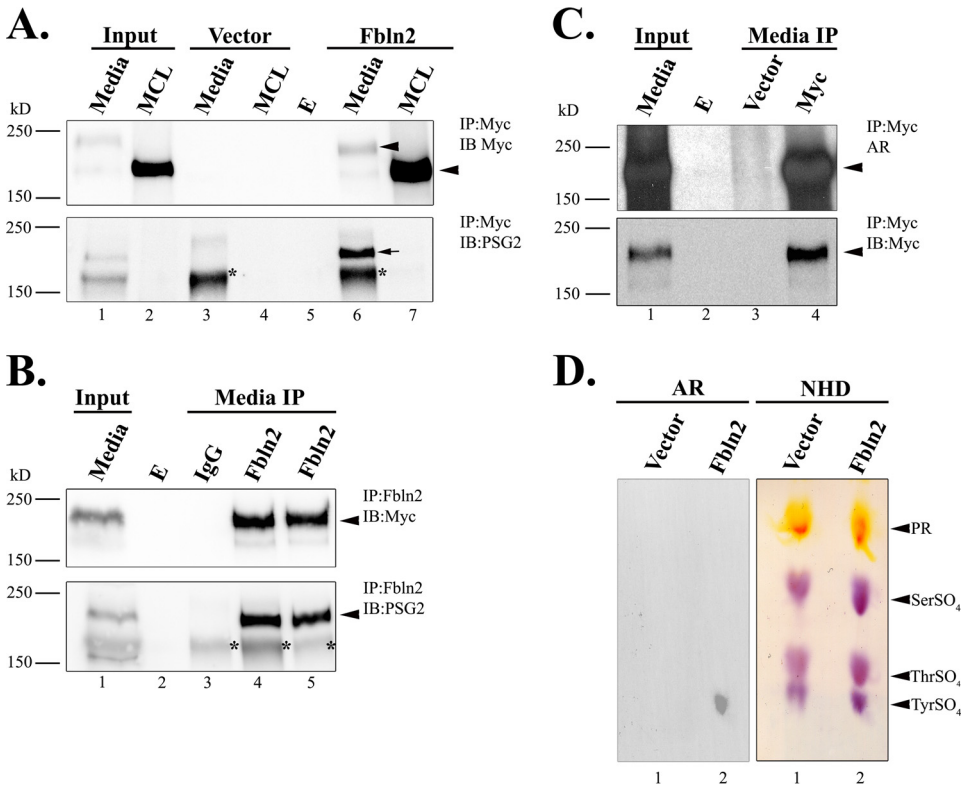

FIGURE 3. **Fbln2 is similarly sulfated *in vitro*.** *A,* immunoprecipitation (*IP*) was performed using anti-Myc antibody on conditioned media (*lanes 3* and *6*) and MCL (*lanes 4* and *7*) of HEK293T cells transiently transfected with either pcDNA 3.1 vector (*lanes 3* and *4*) or recombinant Myc-tagged Fbln2 clone (*lanes 6* and *7*). The immunoprecipitants were fractionated and immunoblotted (*IB*) with anti-Myc antibody and PSG2 antibody. *Arrowheads* point to the two isoforms of Fbln2 identified in the media and MCL fraction (*lanes 6* and *7*). Bands marked with *asterisks* are nonspecific bands that are immunoprecipitated from the media with either pcDNA 3.1 vector or Fbln2. *Lane 5* is an empty lane (*E*). *Arrow* points to sulfated fibulin 2 band. *B,* immunoprecipitation was performed on media from HEK293T cells transiently transfected with Myc-tagged Fbln2 clone. The conditioned media from two independently transfected samples were immunoprecipitated with either rabbit IgG (*lane 3*) or anti-Fbln2 antibody (*lanes 4* and *5*) and immunoblotted with anti-Myc antibody or PSG2. *Arrowheads* point to the 195 kDa Fbln2 isoform in the media. Bands marked with *asterisks* are nonspecific bands that are immunoprecipitated from the media. *Lane 2* is an empty lane. *C,* HEK293T cells were transiently transfected with Myc-tagged Fbln2 clone or vector and grown in the presence of radioactive sulfate. Vector-conditioned media (*lane 3*) or Fbln2-transfected media (*lane 4*) were used for immunoprecipitation with anti-Myc antibody. Following SDS-PAGE and transfer to PVDF membrane, blots were coupled to x-ray film overnight to produce an autoradiogram (*AR*). The blots were then probed with anti-Myc antibody (*lower panel*). *Arrowheads* point to the 195-kDa Fbln2 isoform in the media. *D,* radiolabeled Fbln2 bands were excised, and alkaline hydrolysis was performed and subjected to TLE on a cellulose plates. TLE plates were sprayed with ninhydrin (*NHD*) to reveal the internal standards followed by exposure to x-ray film (autoradiogram (*AR*) to reveal the presence of radioactive tyrosine sulfate present in the radiolabeled Fbln2 recombinant protein immunoprecipitated with anti-Myc antibody (*lane 2*) but not in the vector-immunoprecipitated lane (*lane 1*).

ing transfection, Fbln2 was immunoprecipitated from the media and MCL fractions with an anti-Myc antibody. The immunoprecipitants were electrophoresed, immunoblotted, and probed with the anti-Myc or PSG2 antibodies (Fig. 3*A*). Immunoblotting the immunoprecipitants from the media and MCL of vector-transfected samples did not identify any Myc-labeled protein (*lanes 3* and *4,* Fig. 3*A*, *IB:Myc*). Myc-labeled Fbln2 was successfully immunoprecipitated from media and MCL samples from Fbln2-transfected cells (*lanes 6* and *7,* Fig. 3*A*, *IB:Myc*). The media of Fbln2-transfected cells mostly expressed the 195-kDa long isoform (*arrowhead, lane 6,* Fig. 3*A*, *IB:Myc*), whereas the MCL samples only expressed the shorter 160-kDa isoform (*lane 7,* Fig. 3*A*, *IB:Myc*). Immunoblotting with PSG2 confirmed that the 195-kDa isoform in the media of Fbln2-transfected cells is tyrosine-sulfated (*arrow, lane 6,* Fig. 3*A*, *IB:PSG2*), but the 160-kDa shorter isoform (only in the MCL) is not (*lane 7,* Fig. 3*A*, *IB:PSG2*). A nonspecific tyrosine-sulfated band that is immunoprecipitated from the media of pcDNA 3.1 vector and Fbln2-transfected cells is shown by an *asterisk* in *lanes 3* and *6* of Fig. 3*A*. This nonspecific band is of a similar size and possibly a similar nature to the nonspecific band recognized by the PSG2 antibody in immunoprecipitants of 661W conditioned media (*asterisk, lanes 4* and *5,* Fig. 2*B*).

To confirm that the Myc-tagged clone was in fact Fbln2, it was immunoprecipitated from the conditioned media of two independent transfectants with either anti-Fbln2 antibody or equivalent amounts of rabbit IgG. Immunoblotting the pulled down product with anti-Myc antibody showed the presence of the Myc tag, hence confirming that the identified 195-kDa band is indeed Myc-tagged Fbln2 (*arrowhead, lanes 4* and *5*, Fig. 3*B*, *IB:Myc*). This protein band was not observed in the IgG immunoprecipitants (*lane 3,* Fig. 3*B*, *IB:Myc*). Furthermore, probing with PSG2 confirmed that the 195-kDa Fbln band in the conditioned media is tyrosine-sulfated *in vitro* (*arrowheads, lanes 4* and *5,* Fig. 3*B*, *IB:PSG2*). No fibulin-2-related PSG2 immunoreactivity was observed in IgG controls (*lane 3,* Fig. 3*B*, *IB:PSG2*). Again, the same nonspecific band is detected in the immunoprecipitants from the media of Fbln2-transfected HEK293T cells (*asterisk, lanes 3–5*, Fig. 3*B*, IB:PSG2).

Although PSG2 recognizes sulfotyrosine residues in many sequence contexts (24, 25), the presence of tyrosine sulfate is

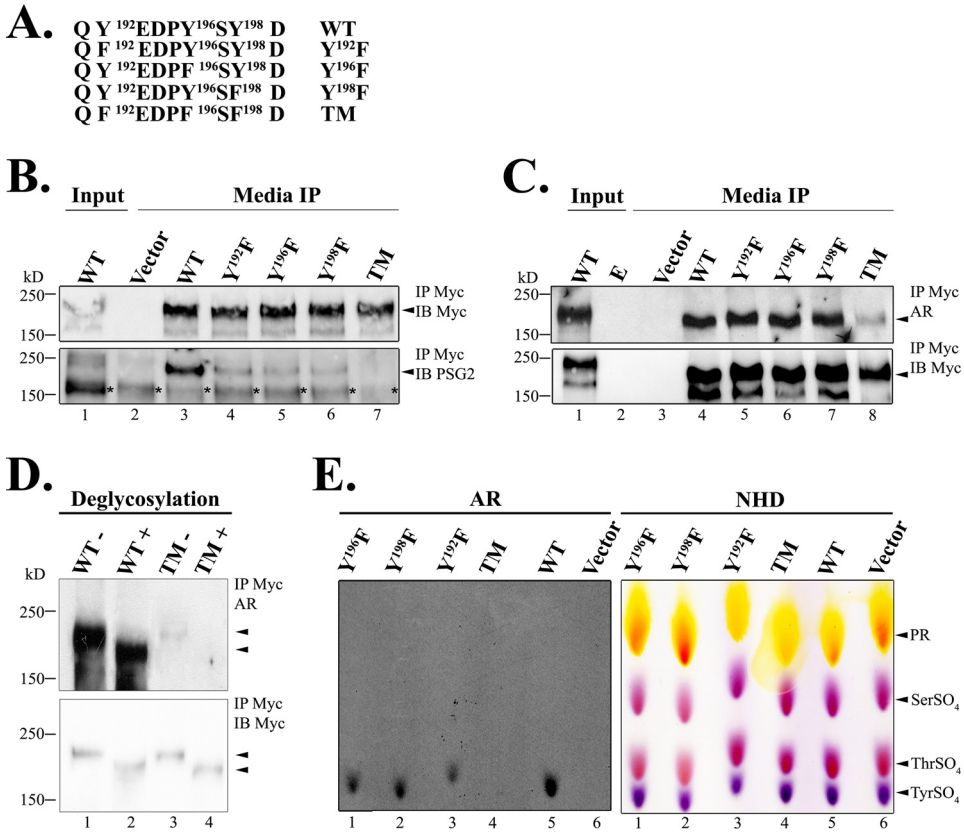

FIGURE 4. **Identification of tyrosine sulfation sites on Fbln2.** *A,* tyrosines identified by Sulfinator as potential sulfation sites include Tyr[192], Tyr[196], and Tyr[198]. Site-directed mutagenesis was performed on Myc-tagged Fbln2 clone (WT) to convert tyrosine residue at positions 192, 196, and 198 to phenylalanines. The Fbln2 clones created were individual tyrosine mutants, Y192F, Y196F, and Y198F, and the triple tyrosine sulfate mutant TM. *B,* HEK293T cells were transiently transfected with pcDNA 3.1 vector (*lane 2*), WT Fbln2 (*lane 3*), single mutants Y192F, Y196F, and Y198F (*lanes 4–6,* respectively), or the triple mutant TM (*lane 7*). The expressed proteins were immunoprecipitated (*IP*) from the conditioned media with anti-Myc antibody, fractionated, and immunoblotted (*IB*) with either anti-Myc antibody or PSG2. *Arrowheads* point to the 195-kDa Fbln2 isoform in the media. Bands marked with *asterisks* are nonspecific bands that are immunoprecipitated from the media. *C,* HEK293T cells were transiently transfected with pcDNA 3.1 vector (*lane 3*), WT Fbln2 (*lane 4*), single mutants Y192F, Y196F, and Y198F (*lanes 5–7,* respectively) and the triple mutant TM (*lane 8*) and were grown in the presence of radioactive sulfate. Conditioned media were used in an immunoprecipitation experiment with anti-Myc antibody followed by SDS-PAGE and immunoblotting. The blots were exposed to x-ray film overnight to produce an autoradiogram (*AR*), followed by immunoblotting with anti-Myc antibody. *D,* radiolabeled WT and TM Fbln2 were immunoprecipitated from conditioned media with anti-Myc antibody and subjected to deglycosylation (*lanes 2* and *4*) or left untreated (*lanes 1* and *3*). The samples were SDS-PAGE fractionated and immunoblotted with anti-Myc antibody. The blots were autoradiograhed and then probed with anti-Myc antibody. The radiolabeled bands were then excised from the blots and counted using liquid scintillation counter. *E,* radiolabeled WT, single mutant clones Y192F, Y196F, and Y198F, and the triple tyrosine sulfate mutant TM proteins were immunoprecipitated from conditioned media, electrophoresed, transferred to PVDF membranes, excised, subjected to alkaline hydrolysis, and analyzed by TLE. Plates were sprayed with ninhydrin (*NHD*), followed by exposure to an x-ray film to produce the autoradiogram.

commonly confirmed after metabolically labeling with radioactive sulfate followed by sulfamino acid analysis. Therefore, Fbln2-transfected HEK293T cells were allowed to grow in the presence of $Na_2{}^{35}SO_4$, and conditioned media were subjected to immunoprecipitation with anti-Myc and then fractionated by SDS-PAGE and autoradiographed. Autoradiographic analysis showed that the immunoprecipitated Fbln2 protein incorporated the radioactive sulfate (*lane 4,* Fig. 3*C*, *AR*), although no label was immunoprecipitated from the vector media (*lane 3,* Fig. 3*C*, *AR*). After autoradiographic analysis, the blot was probed with anti-Myc antibody, which confirmed that the radioactive band is the 195-kDa isoform of Fbln (*lane 4,* Fig. 3*C*, *IB:Myc*). The radiolabeled Fbln2 band and an equivalent area of the membrane from the vector immunoprecipitated lane (*lane 3,* Fig. 3*C*) were cut out and subjected to barium hydroxide hydrolysis followed by TLE analysis using sulfated amino acids as standards (Fig. 3*D*). The co-localization of the radioactive tyrosine sulfate from Fbln2 hydrolysates (*lane 2,* Fig. 3*D*, *AR*) with the nonradioactive tyrosine sulfate standard detected by ninhydrin staining of the TLE plate (*lane 2,* Fig. 3*D*, *NHD*) confirmed the presence of tyrosine sulfate in Fbln2. There was no tyrosine sulfate signal detected in the vector hydrolysates (*lane 1,* Fig. 3*D*, *AR*).

Fibulin 2 Is Sulfated at Tyrosines Residues 192, 196, and 198—As it has been confirmed that Fbln2 is sulfated, it became necessary to identify the target tyrosine(s). The sulfotyrosine predicting program "Sulfinator" (40) identified residues 192, 196, and 198 as potential sites of tyrosine sulfation on Fbln2. Therefore, site-directed mutagenesis was performed on a Myc-tagged Fbln2 clone (WT) to generate four independent mutants. Single mutants, Y192F, Y196F, or Y198F had the individual tyrosine residues at 192, 196, and 198 mutated to phenylalanines (Fig. 4*A*), respectively. A TM was also generated that had all three potential tyrosine residues (192, 196, and 198) mutated to phenylalanines (Fig. 4*A*). All clones as well as pcDNA 3.1 only (vector) were independently transfected into HEK293T cells, and

products were immunoprecipitated from conditioned media with an anti-Myc antibody. Immunoprecipitants were electrophoresed and immunoblotted with anti-Myc and PSG2 antibodies. As shown in Fig. 4*B* (*lanes 3–7*), equivalent levels of all the different recombinant proteins (mutants and wild-type) were pulled down, whereas no Myc reactivity was observed in immunoprecipitants from vector transfectants (*lane 2,* Fig. 4*B*, *IB:Myc*). Immunoblotting with PSG2 demonstrated that the WT clone had the most prominent tyrosine sulfate signal (*arrowhead, lane 3,* Fig. 4*B*, *IB:PSG2*). Each of the single mutants (Y192F, Y196F, or Y198F) showed a reduced tyrosine sulfate signal (*arrowhead, lanes 4–6,* Fig. 4*B*, *IB:PSG2*), although no signal was detected for the TM. A nonspecific protein band was detected in all lanes of the immunoblot (*asterisk, lanes 2–7,* Fig. 4*B*, *IB:PSG2*).

To confirm that the lack of tyrosine sulfate recognition by PSG2 of the TM clone was due to the fact that only three tyrosine sulfate residues (192, 196, and 198) existed in Fbln2, all independent mutant clones along with WT and vector were transiently transfected into HEK293T, and cells were grown in the presence of $Na_2{}^{35}SO_4$. Media from these clones were immunoprecipitated with an anti-Myc antibody. Autoradiographic analysis showed that equivalent radioactivity levels were incorporated by WT and single mutants, although slightly less radioactivity was incorporated by the TM clones (*arrowhead, lanes 4–8,* Fig. 4*C*, *AR*), and no radioactivity was incorporated into vector-transfected samples (*lane 3,* Fig. 4*C*, *AR*). To further confirm that the radioactive immunoprecipitants are Fbln2, blots were probed with anti-Myc antibody, which showed that comparable levels of protein were immunoprecipitated from the media (*lanes 4–8,* Fig. 4*C*, *IB:Myc*). Our data suggest that comparable levels of ^{35}S incorporated in the WT and single mutant clones are due to the fact that Fbln2 is a glycoprotein, and carbohydrates are also sulfated (41). In addition, Fbln2 has been shown to contain four *N*-linked glycosylation residues at the N-terminal end of the protein (23). To prove that carbohydrates are sulfated in WT and TM Fbln2 clones, we again radiolabeled WT and TM Fbln2. One set of WT and TM was subjected to deglycosylation, and another set was left untreated. An ~15-kDa drop in size after deglycosylation of WT and TM Fbln2 proved the presence of carbohydrate residues in the protein (*lanes 2* and *4*, Fig. 4*D*). The radiolabeled bands were cut out and counted by liquid scintillation. Counting showed that deglycosylation of WT and TM Fbln2 decreased the incorporation of the ^{35}S label (3.1×10^{-5} dpm/Fbln2 pixel for nontreated WT Fbln2 *versus* 1.55×10^{-5} dpm/Fbln2 pixel for deglycosylated WT Fbln2 and 1.04×10^{-5} dpm/Fbln2 pixel for nontreated TM Fbln2 *versus* 0.5×10^{-5} dpm/Fbln2 pixel for deglycosylated TM Fbln2).

In addition, to distinguish between carbohydrate sulfation *versus* tyrosine sulfation, the radiolabeled Fbln2 bands of WT, single mutants, and TM Fbln2 were subjected to barium hydroxide hydrolysis (Fig. 4*E*). Barium hydroxide causes the hydrolysis of peptide bonds and the alkali-labile sulfated carbohydrate residues in glycoproteins to be precipitated as barium sulfate. This leaves the tyrosine-sulfated residue intact, which is then identified by co-localization with a tyrosine sulfate standard after neutralization and thin layer electrophoresis analysis

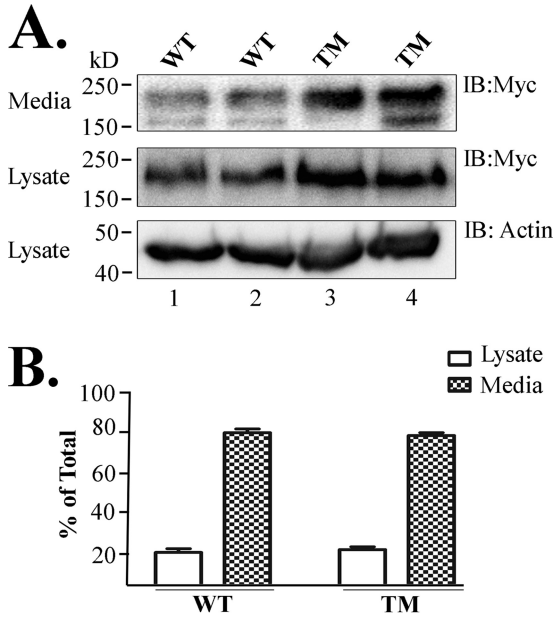

FIGURE 5. **Tyrosine sulfation is not a prerequisite for secretion of Fbln2.** *A,* 15-μl aliquots of conditioned media or cell lysates from two independent permanent transfectants of WT Fbln2 (*lanes 1* and *2*) were compared with two independent permanent transfectants of TM (*lanes 3* and *4*) for the amount of Fbln2 secreted in the media *versus* cytoplasmic lysate fraction. Conditioned media or lysate fractions were subjected to SDS-PAGE and then immunoblotted (*IB*) with anti-Myc antibody. The lysates were also immunoblotted with anti-actin antibody to demonstrate that equivalent amounts were loaded in each lane. *B,* densitometric analysis of data obtained in *A* were plotted using GraphPad Prism. Results present the mean values (± S.E.). Statistical significances were calculated using one-way ANOVA using Bonferroni post-tests. Results were obtained from three independent experiments.

(42). As shown in Fig. 4*E*, radioactive spots were detected in the WT clone (*lane 5,* Fig. 4*E*, *AR*) and all of the single mutants (*lanes 1–3,* Fig. 4*E*, *AR*) but not in the TM or vector clone (*lanes 4* and *6,* Fig. 4*E*, *AR*). This conclusively demonstrates that the three tyrosines (192, 196, and 198) are the only sites of tyrosine sulfation in Fbln2.

Tyrosine Sulfation of Fibulin 2 Does Not Affect Its Secretion—Because Fbln2 is a secreted protein, and tyrosine sulfation is a post-translational modification found mainly in secreted proteins (43), the role of sulfation in the secretion of Fbln2 was investigated. For this purpose, two independent permanent transfectants of either WT or TM Fbln2 were used. Fbln2 protein levels in the media and lysates of tyrosine-sulfated WT (*lanes 1* and *2,* Fig. 5*A*) and nontyrosine-sulfated TM clones (*lanes 3* and *4*, Fig. 5*A*) were compared by immunoblotting with an anti-Myc antibody. Quantitative analysis of the immunoblots presented in Fig. 5*A* showed that both WT and TM secreted ~80% of total expressed Fbln2 in the media fraction, although ~20% of it was sequestered in the cytoplasmic lysate fraction (Fig. 5*B*). The similar distribution of tyrosine-sulfated WT or unsulfated Fbln2 TM clones suggests that sulfation plays no if any role in Fbln2's secretion.

Sulfation Is Involved in the Growth Inhibitory Role of Fibulin 2—It has been previously shown that Fbln2 slows growth rate and cell migration in nasopharyngeal carcinoma cell lines (17). To investigate the growth regulatory role of the tyrosine sulfation of Fbln2, growth curves were generated for permanent transfectants independently expressing empty vector, WT,

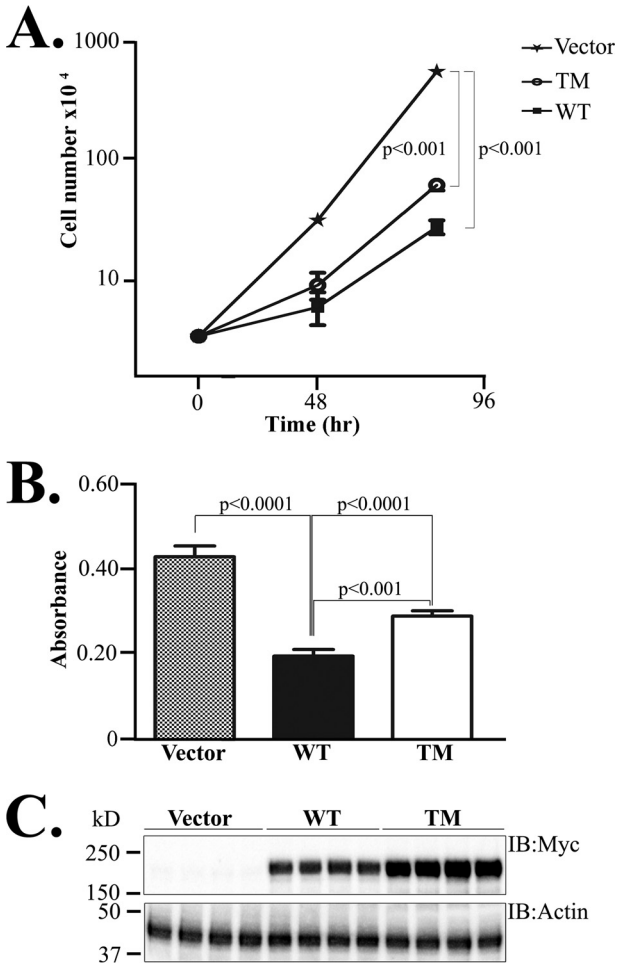

FIGURE 6. **Role of sulfation in fibulin 2 regulation of cellular growth and migration.** *A,* growth suppression by Fbln2. Cell growth of two independent permanent transfectants of pcDNA3.1 vector, WT Fbln2, and TM Fbln2 were compared at 48 and 96 h after initially plating 5×10^4 cells on day 0. Statistical significance was calculated using two-way ANOVA analysis using Bonferroni post-tests. Results present the mean values (± S.E.). Growth curves are plotted on a logarithmic scale. Results were obtained from three independent experiments. *B, in vitro* migration assays were used to compare two permanent transfectants of pcDNA3.1 vector, WT Fbln2, and TM Fbln2 clones after preincubating cells with 2 μg/ml mitomycin C for 45 min. Twenty four hours after plating, the degree of cell migration was assessed as described under "Experimental Procedures." Statistical significance was calculated using one-way ANOVA analysis using Bonferroni post-tests. Results present the mean values (± S.E.). The experiment was performed three times. *C,* to compare the levels of recombinant Fbln2 and actin levels in the permanent transfectants, 50 μg of protein were electrophoresed and immunoblotted (*IB*) using anti-Myc antibody and anti-actin antibody. The experiment was performed three times.

or TM Fbln2s. Cell numbers were counted 48 and 96 h post-plating of 5×10^4 cells on day 0 (Fig. 6*A*). Comparing the growth curves of two independent clones of each vector shows that expression of WT and TM Fbln2 inhibited growth by 64 and 54%, respectively, after 48 h in comparison with vector transfectants (Fig. 6*A*). Comparing the curves of WT and TM Fbln2 at 48 h showed insignificant differences in growth between them. However, at 96 h post-plating, nontyrosine-sulfated TM Fbln2 inhibited growth by 74%, whereas WT Fbln2 inhibited growth by 84% (Fig. 6*A*) compared with the vector transfectants. There was also a significant difference in the growth of WT and TM Fbln2 after 96 h, with the WT Fbln2 inhibiting growth by 39% more than the TM Fbln2 ($p < 0.01$, Fig. 6*A*). These data suggest that although tyrosine sulfation plays a role in the growth inhibitory characteristics of Fbln2, it is not the sole determinant.

Because Fbln2 has previously been shown to have an anti-migratory function in many cell types (16, 17, 44), the role of Fbln2 in the migratory capabilities of the permanent transfectants was investigated using the Transwell system (45) and two independent permanent transfectants expressing vector, WT, or TM Fbln2s. Cells were incubated with 2 μg/ml mitomycin C for 45 min, a dose established to be sufficient to inhibit cell division (data not shown).

Fig. 6*B* shows that WT inhibited migration by 54% compared with vector ($p < 0.0001$), and TM Fbln2 inhibited cell migration by 42% compared with vector (Fig. 6*B*, $p < 0.0001$). In addition, the WT inhibited cell migration by 31% compared with TM Fbln2 ($p < 0.001$, Fig. 6*B*). Because the TM clones expressed higher levels (~2.36) of Myc-tagged Fbln2 compared with the WT clones (Fig. 6*C*), it is reasonable to suggest that the unsulfated TM Fbln2 is not as efficient as WT Fbln2 in inhibiting the migratory capabilities of the cell.

Fibulin 2 Is Up-regulated Following Experimental Retinal Detachment—It has been previously shown that Fbln2 expression can be induced in response to injury in skin, aorta, and liver (5, 46, 47). Furthermore, Farjo *et al.* (21) showed that Fbln2 transcripts increased in the retina following experimental retinal detachment (ERD). To determine whether Fbln2 protein is up-regulated as a result of injury from the needle penetrating the eye, sham injections were performed on the eyes of mice by inserting a needle through the sclera but not penetrating the subretinal space. Levels of Fbln2 were examined at 8, 24, 72, and 168 h after injury. Levels of Fbln2 in the PECS were not significantly changed under these conditions compared with un-injected controls (*lanes 1–5,* Fig. 7, *A* and *B*).

To study the Fbln2 levels in response to ERD and to also determine RPE's response to injury, experimental retinal detachments were induced in mice, and levels of Fbln2 were determined in the retina and RPE.

Although levels of Fbln2 were not significantly changed in the PECS at 8 and 24 h after ERD (*lanes 1–7,* Fig. 7, *C*, *D*, and *E*), at 72 h post-ERD Fbln2 was significantly up-regulated (compare *lanes 1–5* with *lanes 6* and *7*, Fig. 7, *C* and *F*). The levels of Fbln2 continue to be significantly up-regulated at 168 h post-ERD compared with controls (compare *lanes 1–5* with *lanes 6* and *7*, Fig. 7, *C* and *G*). Fbln2 expression was not changed in retinal extracts at all time points tested (data not shown).

Because Fbln2 is an ECM protein expressed in RPE and Bruch membrane (Fig. 1) and has been shown to be a pro-adherent protein (48), the ability of ARPE19 cell, a human RPE cell line (27), to adhere to purified Fbln2 was tested. For this purpose, WT Fbln2 was purified from conditioned media of permanent transfectants using anti-Myc-agarose beads. Conditioned media from vector permanent transfectants similarly isolated served as a negative control. ARPE19 adherence in presence of Fbnc was used as a positive control. Adherence assays showed that a significantly higher number of ARPE19 cells were able to adhere to immobilized WT Fbln2 (Fig. 8*A*, $p < 0.0025$) and Fbnc (Fig. 8*A*, $p < 0.0001$), compared with a BSA control.

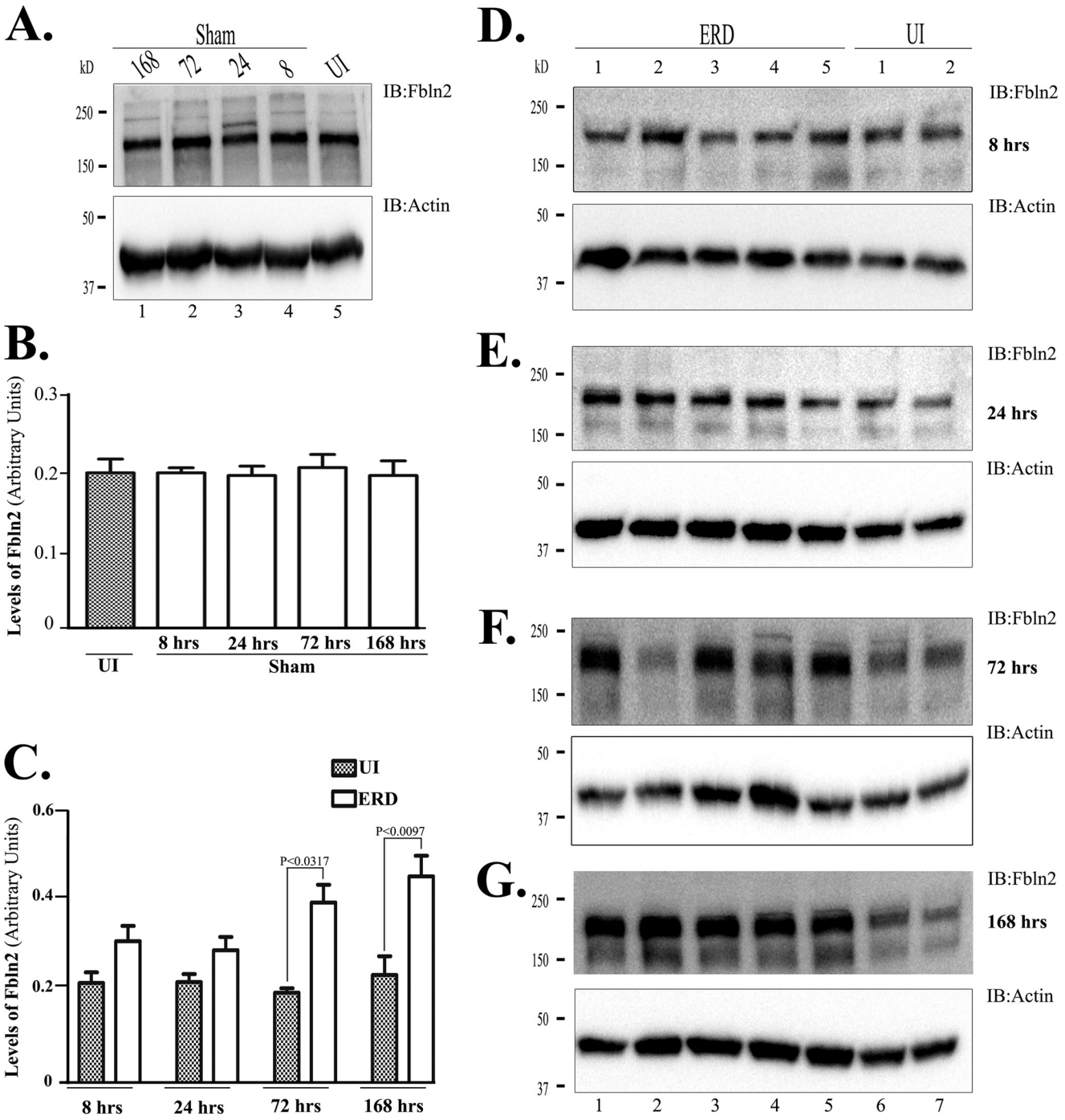

FIGURE 7. **Fbln2 is up-regulated following experimental retinal detachment.** *A,* sham treatment was induced in C57BL/6 mice by inserting a needle through the sclera without entering the subretinal space. PECS were harvested after 8, 24, 72, and 168 h after detachment. Fifty μg of protein from PECS at each time point along with PECS from uninjected (*UI*) mice were separated by SDS-PAGE and immunoblotted (*IB*) with anti-Fbln2 and actin antibodies. *B,* protein expression was quantitated using the Kodak Molecular Imaging software version 4, and the net intensity values were obtained for Fbln2 and actin immunoblots, and Fbln2 values were divided by the values for actin to get "levels of Fbln2." Statistical significances were calculated using one-way ANOVA analysis using Bonferroni post-tests. Results present the mean values (± S.E.). ERD was induced in C57BL/6 mice by injecting 1 μl of saline, and then PECSs were harvested after 8, 24, 72, and 168 h after detachment. *C,* protein expression was quantitated for ERD PECS and uninjected controls using the Kodak Molecular Imaging software version 4, and the net intensity values were obtained for Fbln2 and actin immunoblots, and Fbln2 values were divided by the values for actin to get levels of Fbln2. Statistical significances were calculated using one-way ANOVA analysis using Bonferroni post-tests. Results present the mean values (± S.E.). Each experiment was performed three times. Fifty μg of protein from PECS at 8 (*D*), 24 (*E*), 72 (*F*), and 168 (*G*) hours post-ERD along with PECS from uninjected mice (*UI*) were electrophoresed by SDS-PAGE and immunoblotted with anti-Fbln2 or anti-actin antibodies. Five independent animals were subjected to ERD, and two animals were uninjected (*UI*). The experiment was performed three independent times.

It was observed that following ERD in rabbits, RPE cells are exposed to numerous cytokines that may modulate their behavior and cause RPE to dissociate from the Bruch membrane and migrate (49). Furthermore, collected subretinal fluid from detached human retinas caused the proliferation and migration of RPE cells (50) in culture. Therefore, the effect of Fbln2 on the

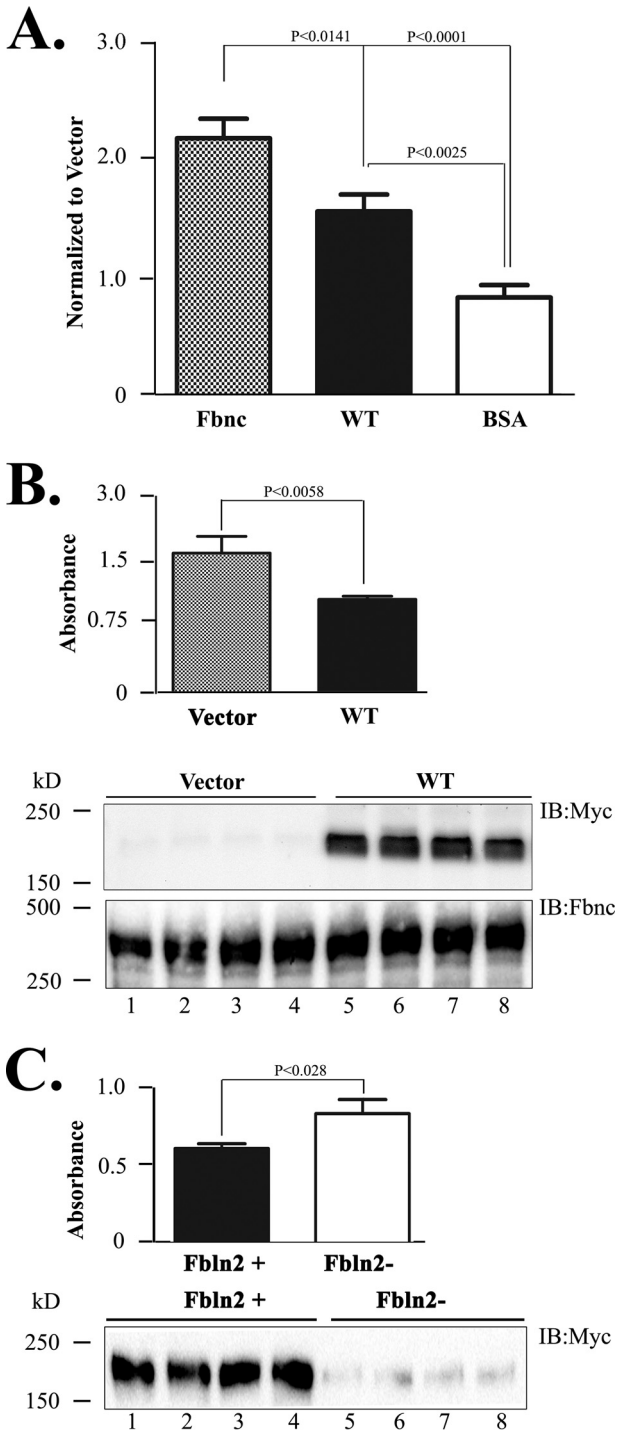

FIGURE 8. *A,* adhesion assays were performed using the ARPE19 cells grown on either purified WT, Fbnc, BSA or eluents obtained from passing media from pcDNA 3.1 transfected cells on the affinity column. About 0.5 μg/ml protein (in the case of pcDNA 3.1 vector, equi-volumes were used) was immobilized on 96-well plates. ARPE19 cells were dissociated and allowed to adhere in the presence of these proteins for 3 h, followed by washing away nonadherent cells, staining the remaining cells with crystal violet, and measuring absorbance at 550 nm. The absorbance of each of the purified protein samples was divided by the absorbance value for the pcDNA 3.1. This resulting "normalized to vector" was plotted using GraphPad Prism. Statistical significance was calculated using one-way ANOVA analysis using Bonferroni post-tests comparing Fbnc and WT Fbln2 to BSA and to each other. Results present the mean values (± S.E.). Each experiment was performed three times in triplicate. *B, in vitro* migration assays were performed comparing the relative migration ability of ARPE19 cells grown in the presence of conditioned media from permanent clones of pcDNA 3.1 vector or WT Fbln2 transfectants. ARPE19 cells were grown in the upper wells of the transwell plates, and conditioned media were placed in the lower chambers. Twenty four hours later, cells that had migrated were stained with crystal violet, and absorbance was measured at 550 nm. Graphs were plotted using GraphPad Prism. Statistical significance was calculated using one-way ANOVAs using Bonferroni post-tests. Results present the mean values (± S.E.). The experiment was done three independent times. *C, in vitro* migration assays were performed comparing the relative migration ability of ARPE19 cells grown in the presence of conditioned media from WT Fbln2 permanent transfectants after immunoprecipitation with IgG (*Fbln2+*) or anti-Myc antibody (*Fbln2−*). ARPE19 cells were grown in the upper wells of the transwell plates, and conditioned media were placed in the lower chambers. Twenty four hours later, cells that had migrated were stained with crystal violet, and absorbance was measured at 550 nm. Graphs were plotted using GraphPad prism. Statistical significance was calculated using one-way ANOVA analysis using Bonferroni post-tests. Results present the mean values (± S.E.).

migratory capabilities of ARPE19 was tested. Absorbance values after 24 h showed that migration of ARPE19 cells was significantly inhibited by media from WT Fbln2 (~33%) (Fig. 8*B*, $p < 0.0058$) compared with ARPE19 cells growing in vector media. To verify that the anti-migratory function was due to WT Fbln2, media from the lower chamber in each Transwell were analyzed by SDS-PAGE followed by immunoblotting with anti-Myc antibody. As shown in Fig. 8*B*, WT Fbln2 was present in the lower Transwell chamber. Immunoblotting for Fbnc was used to demonstrate that equivalent amounts of conditioned media were used (Fig. 8*B*, *IB:Fbnc*). Results presented in Fig. 8*B* show that the suppression of migration of ARPE19 is likely due to the presence of Fbln2. To support the previous conclusion, an equi-volume of conditioned media from WT Fbln2 permanent transfectants was subjected to immunoprecipitation with anti-Myc or mouse IgG antibodies. Because WT Fbln2 is Myc-tagged, it is immunodepleted by immunoprecipitation with anti-Myc antibody. Fig. 8*C* shows the presence of Fbln2 in the conditioned media after mouse IgG immunoprecipitation as a control (Fig. 8*C*, *Fbln2+*) and 3-fold reduction after anti-Myc immunoprecipitation (*Fbln2−*). Migration of ARPE19 cells was analyzed in the presence and absence of Fbln2-immunodepleted media. Migration was inhibited by 26% (Fig. 8*C, top,* $p < 0.028$) in the presence of Fbln2. This result confirms that the presence of Fbln2 was responsible for inhibition of migration of ARPE19 cells.

DISCUSSION

In the course of identifying tyrosine-sulfated proteins in ocular tissues using a PSG2 affinity column (24) followed by tandem mass spectrometry, Fbln2 was detected. Because Fbln2 has not been studied in any detail in the eye, we focused our studies on determining its cellular localization, its potential function in the eye, and the role of tyrosine sulfation in its function. In the mouse eye, Fbln2 was detected mainly in the RPE, BrM, and choriocapillaries. In the photoreceptor cell line 661W, Fbln2 existed in two isoforms, a 195-kDa isoform and a 160-kDa isoform. The presence of the 195- and 160-kDa isoforms of Fbln2 has been reported previously. Only the 195-kDa isoform has been shown in breast cancer cell lines (16), Schlemm canal cells (51), mouse ear (52), and aorta (53), although both the 195- and 160-kDa isoforms have been reported in nasopharyngeal cell lines (17) and mouse fibroblasts (32).

Sequence analysis of Fbln2 revealed four potential *N*-linked glycosylation sites (23), and so the 195-kDa isoform is likely a

glycosylated isoform of Fbln2, whereas the 160-kDa isoform represents the nonglycosylated immature isoform. In addition, it is the large 195-kDa isoform of Fbln2 that is present outside the cell as determined by trypsin accessibility of this isoform in 661W, whereas the 160-kDa isoform is protected from trypsin suggesting that it is present inside the cell. The 195-kDa isoform itself is present in two fractions as follows: a tyrosine-sulfated form in the media and an unsulfated form in the MCL fraction. One possibility for the presence of the two forms could be due to the ability of the 661W cells to produce the two forms independently. Alternatively, the unsulfated form may result from specific sulfatase action post-secretion. The absence of any ECM-based tyrosine sulfatase activity favors the former possibility. Regardless, the presence of the two forms emphasizes the importance of Fbln2 and the role tyrosine sulfation can play in the function of a protein.

Although tyrosine sulfation has been shown to influence the ability of the cell to secrete some proteins (54, 55), the lack of tyrosine sulfation of Fbln2 did not affect its secretion. Both the tyrosine-sulfated and unsulfated forms of Fbln2 inhibited growth compared with vector-transfected permanent transfectants. However, the tyrosine-sulfated form of Fbln2 was additionally able to inhibit growth compared with the unsulfated isoform by 39% at 96 h, suggesting a role of Fbln2's sulfation in regulating cellular growth. Such a role in regulating growth has been previously studied in the glycosaminoglycans in the ECM, where it has been shown that sulfation of glycosaminoglycans is important for the sequestration and regulation of growth factors and associated signaling (56–58). Experimental desulfation resulted in decreased sequestration and enhanced growth factor signaling (59). It is conceivable that such effects could also be assigned to tyrosine sulfation of a protein.

Tyrosine-sulfated Fbln2, reduced migration of HEK293T cells by 54%, and the unsulfated counterpart was able to reduce the migration rate by 42% compared with the vector control. When comparing the migration differences between two independent WT Fbln2-expressing permanent clones that only differ in expression levels, we observed a 68% decrease of migration with a 2-fold increase in WT-fibulin 2 (data not shown). Comparing the tyrosine-sulfated Fbln2 to the non-tyrosine-sulfated TM showed a 31% inhibition of cell migration by the WT Fbln2. Moreover, the higher levels of Fbln2 expressed by the non-tyrosine-sulfated TM clone compared with the tyrosine-sulfated WT clones indicates that removing tyrosine sulfation from Fbln2 removes anti-migratory effects of WT Fbln2. The ability of Fbln2 to reduce growth rate and migration was described previously in breast and nasopharyngeal cancer cells (16, 17). This may be due to the fact that Fbln2 is an ECM protein that forms molecular bridges by binding other ECM proteins such as fibronectin, laminins, perlecans, versicans, aggrecan, and nidogens (60–64). In doing so, it may sequester growth factors essential for growth and migration of the cell. Future studies will address whether we observe a difference in growth factor sequestration between wild-type and unsulfated Fbln2s.

One observation in our studies is that the outcome of eliminating tyrosine sulfation resulted in a 39% increase in growth rate and a 31% increase in migration rate compared with its tyrosine-sulfated counterpart. Other studies where tyrosine sulfation was eliminated as in the protein P-selectin glycoprotein ligand-1 showed that elimination of tyrosine sulfation reduces but does not eliminate binding and rolling on endothelial cells (65, 66). Similarly, studies on Factor VIII, where a naturally occurring mutation changes the tyrosine sulfate residue to phenylalanine, moderately reduces binding to the von Willebrand factor and causes mild hemophilia (67). Studies on the chemokine receptor CCR3 that contains two tyrosine sulfate residues have shown that elimination of tyrosine sulfation from both residues or one residue does not eliminate binding to its ligands eotaxin-1, -2, or -3, but it only modulates the selectivity of the receptor to the three chemokines (68). Therefore, our studies and other studies suggest that tyrosine sulfation is required for optimum function, and lack of it does not altogether eliminate the function.

Retinal detachment is the physical separation of the RPE from the outer segments of photoreceptors. It is a common occurrence as a consequence of old age, trauma, and cataract surgery and as a complication of diseases such as proliferative diabetic retinopathy, proliferative vitreoretinopathy, and uveitis (69). Large population-based studies put the annual incidence of retinal detachment around 1 in 10,000 people and a lifetime risk of 3% at the age of 85 years (70, 71). Retinal detachment can lead to the exposure of the quiescent RPE cells (72) to multiple cytokines, which may modulate their behavior and cause them to dissociate from the Bruch membrane (73), undergo major morphological changes on the apical surface (74), or change their morphology from flat cuboid to columnar in appearance and enlarge in size (75). RPE proliferation and migration after retinal detachment has been observed in many species (49, 50, 76, 77). An extreme condition that results due to retinal detachment occurs during proliferative vitreoretinopathy, where RPE cells trans-differentiate into myofibroblasts and proliferate into the vitreous humor to form sub-retinal membranes (78, 79). It is feasible that one of the reasons most RPE cells adhere back to the photoreceptor layer and do not migrate following detachment is due to up-regulation of anti-proliferative and anti-migratory proteins such as Fbln2. This is supported by our findings that Fbln2 is up-regulated in the PECS fractions at 72 and 168 h post-ERD. Studies on *Efemp1* (Fbln 3) knock-in mice showed that the R345W mutation leads to the photoreceptor outer segment detachment from the RPE (36). Therefore, considering the function of Fbln2 as an adherent ECM protein and its anti-migratory capabilities, it is likely that it may have a similar role in RPE-photoreceptor adherence. Our future studies will analyze the effects of endogenous fibulin 2 on RPE migration and adhesion by studying its effect in the fibulin $2^{-/-}$ mice.

Previous studies using surface plasma resonance assays have shown that mouse Fbln2, with an 'RGD' motif in the N-terminal cysteine-free domain, can adhere to cells by direct binding to multiple integrins (48). It can also modulate the adhesiveness of the ECM to the cells by binding other 'RGD' containing ECM proteins such as collagen IV, fibronectin and laminin (60, 62). Our *in vitro* adhesion assays show that ARPE19 cells can adhere to purified Fbln2. Future studies will focus on identifying the RPE integrins involved in this process.

Current therapies to treat retinal detachment involve surgical and nonsurgical techniques. The nonsurgical procedures involve cryotherapy using a freezing probe to seal the retina to the RPE; diathermy uses heat to seal the retina to the RPE; for laser therapy and pneumatic retinopexy, a gas bubble is introduced to allow the retina to float back into position, after which the hole is sealed with a laser. Surgical procedures involve scleral buckle surgery, where a silicon band is sewn to the sclera and pulled tight, then the sclera buckles and causes the retina to stick back to the RPE and vitrectomy, and then the scar tissue that is responsible for pulling the retina from the RPE is removed.

In summary, this report demonstrates a role for the ECM protein Fbln2 in ocular tissues and provides evidence for its up-regulation following retinal detachment. A more definitive role of Fbln2 in retinal detachments will be addressed in future studies involving the use of Fbln2 knock-out animals.

Acknowledgments—We thank Dr. Mon-Li Chu (Thomas Jefferson University) for kindly providing us with the anti-Fbln2 antibody. We are grateful for technical assistance provided by Robert Hamilton, Michael Stuck, and Joseph Siefert.

REFERENCES

1. Sicot, F. X., Tsuda, T., Markova, D., Klement, J. F., Arita, M., Zhang, R. Z., Pan, T. C., Mecham, R. P., Birk, D. E., and Chu, M. L. (2008) Fibulin-2 is dispensable for mouse development and elastic fiber formation. *Mol. Cell. Biol.* **28,** 1061–1067
2. Dietrich-Ntoukas, T., Hofmann-Rummelt, C., Kruse, F. E., and Schlötzer-Schrehardt, U. (2012) Comparative analysis of the basement membrane composition of the human limbus epithelium and amniotic membrane epithelium. *Cornea* **31,** 564–569
3. Loveland, K., Schlatt, S., Sasaki, T., Chu, M. L., Timpl, R., and Dziadek, M. (1998) Developmental changes in the basement membrane of the normal and hypothyroid postnatal rat testis: segmental localization of fibulin-2 and fibronectin. *Biol. Reprod.* **58,** 1123–1130
4. Miosge, N., Götz, W., Sasaki, T., Chu, M. L., Timpl, R., and Herken, R. (1996) The extracellular matrix proteins fibulin-1 and fibulin-2 in the early human embryo. *Histochem. J.* **28,** 109–116
5. Hunzelmann, N., Nischt, R., Brenneisen, P., Eickert, A., and Krieg, T. (2001) Increased deposition of fibulin-2 in solar elastosis and its colocalization with elastic fibres. *Br. J. Dermatol.* **145,** 217–222
6. Yanagisawa, H., Schluterman, M. K., and Brekken, R. A. (2009) Fibulin-5, an integrin-binding matricellular protein: its function in development and disease. *J. Cell Commun. Signal.* **3,** 337–347
7. de Vega, S., Iwamoto, T., and Yamada, Y. (2009) Fibulins: multiple roles in matrix structures and tissue functions. *Cell. Mol. Life Sci.* **66,** 1890–1902
8. Argraves, W. S., Greene, L. M., Cooley, M. A., and Gallagher, W. M. (2003) Fibulins: physiological and disease perspectives. *EMBO Rep.* **4,** 1127–1131
9. Lotery, A. J., Baas, D., Ridley, C., Jones, R. P., Klaver, C. C., Stone, E., Nakamura, T., Luff, A., Griffiths, H., Wang, T., Bergen, A. A., and Trump, D. (2006) Reduced secretion of fibulin 5 in age-related macular degeneration and cutis laxa. *Hum. Mutat.* **27,** 568–574
10. Nakamura, T., Lozano, P. R., Ikeda, Y., Iwanaga, Y., Hinek, A., Minamisawa, S., Cheng, C. F., Kobuke, K., Dalton, N., Takada, Y., Tashiro, K., Ross, Jr, J., Honjo, T., and Chien, K. R. (2002) Fibulin-5/DANCE is essential for elastogenesis *in vivo*. *Nature* **415,** 171–175
11. Hucthagowder, V., Sausgruber, N., Kim, K. H., Angle, B., Marmorstein, L. Y., and Urban, Z. (2006) Fibulin-4: a novel gene for an autosomal recessive cutis laxa syndrome. *Am. J. Hum. Genet.* **78,** 1075–1080
12. Debeer, P., Schoenmakers, E. F., Twal, W. O., Argraves, W. S., De Smet, L., Fryns, J. P., and Van De Ven, W. J. (2002) The fibulin-1 gene (FBLN1) is disrupted in a t(12;22) associated with a complex type of synpolydactyly. *J. Med. Genet.* **39,** 98–104
13. Hill, V. K., Hesson, L. B., Dansranjavin, T., Dallol, A., Bieche, I., Vacher, S., Tommasi, S., Dobbins, T., Gentle, D., Euhus, D., Lewis, C., Dammann, R., Ward, R. L., Minna, J., Maher, E. R., Pfeifer, G. P., and Latif, F. (2010) Identification of 5 novel genes methylated in breast and other epithelial cancers. *Mol. Cancer* **9,** 51
14. Dunwell, T. L., Hesson, L. B., Pavlova, T., Zabarovska, V., Kashuba, V., Catchpoole, D., Chiaramonte, R., Brini, A. T., Griffiths, M., Maher, E. R., Zabarovsky, E., and Latif, F. (2009) Epigenetic analysis of childhood acute lymphoblastic leukemia. *Epigenetics* **4,** 185–193
15. Alcendor, D. J., Knobel, S., Desai, P., Zhu, W. Q., and Hayward, G. S. (2011) KSHV regulation of fibulin-2 in Kaposi's sarcoma: implications for tumorigenesis. *Am. J. Pathol.* **179,** 1443–1454
16. Yi, C. H., Smith, D. J., West, W. W., and Hollingsworth, M. A. (2007) Loss of fibulin-2 expression is associated with breast cancer progression. *Am. J. Pathol.* **170,** 1535–1545
17. Law, E. W., Cheung, A. K., Kashuba, V. I., Pavlova, T. V., Zabarovsky, E. R., Lung, H. L., Cheng, Y., Chua, D., Lai-Wan Kwong, D., Tsao, S. W., Sasaki, T., Stanbridge, E. J., and Lung, M. L. (2012) Anti-angiogenic and tumor-suppressive roles of candidate tumor-suppressor gene, Fibulin-2, in nasopharyngeal carcinoma. *Oncogene* **31,** 728–738
18. Stone, E. M., Lotery, A. J., Munier, F. L., Héon, E., Piguet, B., Guymer, R. H., Vandenburgh, K., Cousin, P., Nishimura, D., Swiderski, R. E., Silvestri, G., Mackey, D. A., Hageman, G. S., Bird, A. C., Sheffield, V. C., and Schorderet, D. F. (1999) A single EFEMP1 mutation associated with both Malattia Leventinese and Doyne honeycomb retinal dystrophy. *Nat. Genet.* **22,** 199–202
19. Stone, E. M., Braun, T. A., Russell, S. R., Kuehn, M. H., Lotery, A. J., Moore, P. A., Eastman, C. G., Casavant, T. L., and Sheffield, V. C. (2004) Missense variations in the fibulin 5 gene and age-related macular degeneration. *N. Engl. J. Med.* **351,** 346–353
20. Fisher, S. A., Rivera, A., Fritsche, L. G., Keilhauer, C. N., Lichtner, P., Meitinger, T., Rudolph, G., and Weber, B. H. (2007) Case-control genetic association study of fibulin-6 (FBLN6 or HMCN1) variants in age-related macular degeneration (AMD). *Hum. Mutat.* **28,** 406–413
21. Farjo, R., Peterson, W. M., and Naash, M. I. (2008) Expression profiling after retinal detachment and reattachment: a possible role for aquaporin-0. *Invest. Ophthalmol. Vis. Sci.* **49,** 511–521
22. Johnson, E. C., Jia, L., Cepurna, W. O., Doser, T. A., and Morrison, J. C. (2007) Global changes in optic nerve head gene expression after exposure to elevated intraocular pressure in a rat glaucoma model. *Invest. Ophthalmol. Vis. Sci.* **48,** 3161–3177
23. Pan, T. C., Sasaki, T., Zhang, R. Z., Fässler, R., Timpl, R., and Chu, M. L. (1993) Structure and expression of fibulin-2, a novel extracellular matrix protein with multiple EGF-like repeats and consensus motifs for calcium binding. *J. Cell Biol.* **123,** 1269–1277
24. Hoffhines, A. J., Damoc, E., Bridges, K. G., Leary, J. A., and Moore, K. L. (2006) Detection and purification of tyrosine-sulfated proteins using a novel anti-sulfotyrosine monoclonal antibody. *J. Biol. Chem.* **281,** 37877–37887
25. Hoffhines, A. J., Jen, C. H., Leary, J. A., and Moore, K. L. (2009) Tyrosylprotein sulfotransferase-2 expression is required for sulfation of RNase 9 and Mfge8 *in vivo*. *J. Biol. Chem.* **284,** 3096–3105
26. Tan, E., Ding, X. Q., Saadi, A., Agarwal, N., Naash, M. I., and Al-Ubaidi, M. R. (2004) Expression of cone-photoreceptor-specific antigens in a cell line derived from retinal tumors in transgenic mice. *Invest. Ophthalmol. Vis. Sci.* **45,** 764–768
27. Dunn, K. C., Aotaki-Keen, A. E., Putkey, F. R., and Hjelmeland, L. M. (1996) ARPE-19, a human retinal pigment epithelial cell line with differentiated properties. *Exp. Eye Res.* **62,** 155–169
28. Shaw, G., Morse, S., Ararat, M., and Graham, F. L. (2002) Preferential transformation of human neuronal cells by human adenoviruses and the origin of HEK293 cells. *FASEB J.* **16,** 869–871
29. Chen, C. A., and Okayama, H. (1988) Calcium phosphate-mediated gene transfer: a highly efficient transfection system for stably transforming cells with plasmid DNA. *BioTechniques* **6,** 632–638
30. Chen, C., and Okayama, H. (1987) High-efficiency transformation of mammalian cells by plasmid DNA. *Mol. Cell. Biol.* **7,** 2745–2752

31. Kanan, Y., Hoffhines, A., Rauhauser, A., Murray, A., and Al-Ubaidi, M. R. (2009) Protein tyrosine-*O*-sulfation in the retina. *Exp. Eye Res.* **89,** 559–567
32. Sasaki, T., Wiedemann, H., Matzner, M., Chu, M. L., and Timpl, R. (1996) Expression of fibulin-2 by fibroblasts and deposition with fibronectin into a fibrillar matrix. *J. Cell Sci.* **109,** 2895–2904
33. Laemmli, U. K. (1970) Cleavage of structural proteins during the assembly of the head of bacteriophage T4. *Nature* **227,** 680–685
34. Al-Ubaidi, M. R., Mangini, N. J., Quiambao, A. B., Myers, K. M., Abler, A. S., Chang, C. J., Tso, M. O., Butel, J. S., and Hollyfield, J. G. (1997) Unscheduled DNA replication precedes apoptosis of photoreceptors expressing SV40 T antigen. *Exp. Eye Res.* **64,** 573–585
35. Sherry, D. M., Murray, A. R., Kanan, Y., Arbogast, K. L., Hamilton, R. A., Fliesler, S. J., Burns, M. E., Moore, K. L., and Al-Ubaidi, M. R. (2010) Lack of protein-tyrosine sulfation disrupts photoreceptor outer segment morphogenesis, retinal function and retinal anatomy. *Eur. J. Neurosci.* **32,** 1461–1472
36. Marmorstein, L. Y., McLaughlin, P. J., Peachey, N. S., Sasaki, T., and Marmorstein, A. D. (2007) Formation and progression of sub-retinal pigment epithelium deposits in Efemp1 mutation knock-in mice: a model for the early pathogenic course of macular degeneration. *Hum. Mol. Genet.* **16,** 2423–2432
37. Westmuckett, A. D., Hoffhines, A. J., Borghei, A., and Moore, K. L. (2008) Early postnatal pulmonary failure and primary hypothyroidism in mice with combined TPST-1 and TPST-2 deficiency. *Gen. Comp. Endocrinol.* **156,** 145–153
38. Nour, M., Quiambao, A. B., Peterson, W. M., Al-Ubaidi, M. R., and Naash, M. I. (2003) P2Y(2) receptor agonist INS37217 enhances functional recovery after detachment caused by subretinal injection in normal and rds mice. *Invest. Ophthalmol. Vis. Sci.* **44,** 4505–4514
39. al-Ubaidi, M. R., Font, R. L., Quiambao, A. B., Keener, M. J., Liou, G. I., Overbeek, P. A., and Baehr, W. (1992) Bilateral retinal and brain tumors in transgenic mice expressing simian virus 40 large T antigen under control of the human interphotoreceptor retinoid-binding protein promoter. *J. Cell Biol.* **119,** 1681–1687
40. Monigatti, F., Gasteiger, E., Bairoch, A., and Jung, E. (2002) The Sulfinator: predicting tyrosine sulfation sites in protein sequences. *Bioinformatics* **18,** 769–770
41. Muthana, S. M., Campbell, C. T., and Gildersleeve, J. C. (2012) Modifications of glycans: biological significance and therapeutic opportunities. *ACS Chem. Biol.* **7,** 31–43
42. Huttner, W. B. (1984) Determination and occurrence of tyrosine *O*-sulfate in proteins. *Methods Enzymol.* **107,** 200–223
43. Moore, K. L. (2003) The biology and enzymology of protein tyrosine *O*-sulfation. *J. Biol. Chem.* **278,** 24243–24246
44. Ström, A., Olin, A. I., Aspberg, A., and Hultgårdh-Nilsson, A. (2006) Fibulin-2 is present in murine vascular lesions and is important for smooth muscle cell migration. *Cardiovasc. Res.* **69,** 755–763
45. Senger, D. R., Perruzzi, C. A., Streit, M., Koteliansky, V. E., de Fougerolles, A. R., and Detmar, M. (2002) The $\alpha(1)\beta(1)$ and $\alpha(2)\beta(1)$ integrins provide critical support for vascular endothelial growth factor signaling, endothelial cell migration, and tumor angiogenesis. *Am. J. Pathol.* **160,** 195–204
46. Piscaglia, F., Dudás, J., Knittel, T., Di Rocco, P., Kobold, D., Saile, B., Zocco, M. A., Timpl, R., and Ramadori, G. (2009) Expression of ECM proteins fibulin-1 and -2 in acute and chronic liver disease and in cultured rat liver cells. *Cell Tissue Res.* **337,** 449–462
47. Tsuda, T., Wu, J., Gao, E., Joyce, J., Markova, D., Dong, H., Liu, Y., Zhang, H., Zou, Y., Gao, F., Miller, T., Koch, W., Ma, X., and Chu, M. L. (2012) Loss of fibulin-2 protects against progressive ventricular dysfunction after myocardial infarction. *J. Mol. Cell. Cardiol.* **52,** 273–282
48. Pfaff, M., Sasaki, T., Tangemann, K., Chu, M. L., and Timpl, R. (1995) Integrin-binding and cell-adhesion studies of fibulins reveal a particular affinity for αIIbβ3. *Exp. Cell Res.* **219,** 87–92
49. Ivert, L., Kjeldbye, H., and Gouras, P. (2002) Long-term effects of short-term retinal bleb detachments in rabbits. *Graefes Arch. Clin. Exp. Ophthalmol.* **240,** 232–237
50. Hackett, S. F., Conway, B. P., and Campochiaro, P. A. (1989) Subretinal fluid stimulation of retinal pigment epithelial cell migration and proliferation is dependent on certain features of the detachment or its treatment. *Arch. Ophthalmol.* **107,** 391–394
51. Perkumas, K. M., and Stamer, W. D. (2012) Protein markers and differentiation in culture for Schlemm's canal endothelial cells. *Exp. Eye Res.* **96,** 82–87
52. Kusubata, M., Hirota, A., Ebihara, T., Kuwaba, K., Matsubara, Y., Sasaki, T., Kusakabe, M., Tsukada, T., Irie, S., and Koyama, Y. (1999) Spatiotemporal changes of fibronectin, tenascin-C, fibulin-1, and fibulin-2 in the skin during the development of chronic contact dermatitis. *J. Invest. Dermatol.* **113,** 906–912
53. Chapman, S. L., Sicot, F. X., Davis, E. C., Huang, J., Sasaki, T., Chu, M. L., and Yanagisawa, H. (2010) Fibulin-2 and fibulin-5 cooperatively function to form the internal elastic lamina and protect from vascular injury. *Arterioscler. Thromb. Vasc. Biol.* **30,** 68–74
54. Kim, T. H., Kim do, H., Nam, H. W., Park, S. Y., Shim, J., and Cho, J. W. (2010) Tyrosylprotein sulfotransferase regulates collagen secretion in *Caenorhabditis elegans*. *Mol. Cells* **29,** 413–418
55. Friederich, E., Fritz, H. J., and Huttner, W. B. (1988) Inhibition of tyrosine sulfation in the trans-Golgi retards the transport of a constitutively secreted protein to the cell surface. *J. Cell Biol.* **107,** 1655–1667
56. Lindahl, U., and Höök, M. (1978) Glycosaminoglycans and their binding to biological macromolecules. *Annu. Rev. Biochem.* **47,** 385–417
57. Zafiropoulos, A., Fthenou, E., Chatzinikolaou, G., and Tzanakakis, G. N. (2008) Glycosaminoglycans and PDGF signaling in mesenchymal cells. *Connect. Tissue Res.* **49,** 153–156
58. Rider, C. C. (2006) Heparin/heparan sulphate binding in the TGF-β cytokine superfamily. *Biochem. Soc. Trans.* **34,** 458–460
59. Lim, J. J., and Temenoff, J. S. (2013) The effect of desulfation of chondroitin sulfate on interactions with positively charged growth factors and upregulation of cartilaginous markers in encapsulated MSCs. *Biomaterials* **34,** 5007–5018
60. Sasaki, T., Göhring, W., Pan, T. C., Chu, M. L., and Timpl, R. (1995) Binding of mouse and human fibulin-2 to extracellular matrix ligands. *J. Mol. Biol.* **254,** 892–899
61. Hopf, M., Göhring, W., Kohfeldt, E., Yamada, Y., and Timpl, R. (1999) Recombinant domain IV of perlecan binds to nidogens, laminin-nidogen complex, fibronectin, fibulin-2 and heparin. *Eur. J. Biochem.* **259,** 917–925
62. Utani, A., Nomizu, M., and Yamada, Y. (1997) Fibulin-2 binds to the short arms of laminin-5 and laminin-1 via conserved amino acid sequences. *J. Biol. Chem.* **272,** 2814–2820
63. Salmivirta, K., Talts, J. F., Olsson, M., Sasaki, T., Timpl, R., and Ekblom, P. (2002) Binding of mouse nidogen-2 to basement membrane components and cells and its expression in embryonic and adult tissues suggest complementary functions of the two nidogens. *Exp. Cell Res.* **279,** 188–201
64. Olin, A. I., Mörgelin, M., Sasaki, T., Timpl, R., Heinegård, D., and Aspberg, A. (2001) The proteoglycans aggrecan and Versican form networks with fibulin-2 through their lectin domain binding. *J. Biol. Chem.* **276,** 1253–1261
65. Rodgers, S. D., Camphausen, R. T., and Hammer, D. A. (2001) Tyrosine sulfation enhances but is not required for PSGL-1 rolling adhesion on P-selectin. *Biophys. J.* **81,** 2001–2009
66. Ramachandran, V., Nollert, M. U., Qiu, H., Liu, W. J., Cummings, R. D., Zhu, C., and McEver, R. P. (1999) Tyrosine replacement in P-selectin glycoprotein ligand-1 affects distinct kinetic and mechanical properties of bonds with P- and L-selectin. *Proc. Natl. Acad. Sci. U.S.A.* **96,** 13771–13776
67. Leyte, A., van Schijndel, H. B., Niehrs, C., Huttner, W. B., Verbeet, M. P., Mertens, K., and van Mourik, J. A. (1991) Sulfation of Tyr1680 of human blood coagulation factor VIII is essential for the interaction of factor VIII with von Willebrand factor. *J. Biol. Chem.* **266,** 740–746
68. Zhu, J. Z., Millard, C. J., Ludeman, J. P., Simpson, L. S., Clayton, D. J., Payne, R. J., Widlanski, T. S., and Stone, M. J. (2011) Tyrosine sulfation influences the chemokine binding selectivity of peptides derived from chemokine receptor CCR3. *Biochemistry* **50,** 1524–1534
69. Kang, H. K., and Luff, A. J. (2008) Management of retinal detachment: a guide for non-ophthalmologists. *BMJ* **336,** 1235–1240
70. Polkinghorne, P. J., and Craig, J. P. (2004) Northern New Zealand Rhegmatogenous Retinal Detachment Study: epidemiology and risk factors.

Clin. Experiment. Ophthalmol. **32,** 159–163
71. Go, S. L., Hoyng, C. B., and Klaver, C. C. (2005) Genetic risk of rhegmatogenous retinal detachment: a familial aggregation study. *Arch. Ophthalmol.* **123,** 1237–1241
72. García, S., López, E., and López-Colomé, A. M. (2008) Glutamate accelerates RPE cell proliferation through ERK1/2 activation via distinct receptor-specific mechanisms. *J. Cell Biochem.* **104,** 377–390
73. Saika, S., Yamanaka, O., Flanders, K. C., Okada, Y., Miyamoto, T., Sumioka, T., Shirai, K., Kitano, A., Miyazaki, K., Tanaka, S., and Ikeda, K. (2008) Epithelial-mesenchymal transition as a therapeutic target for prevention of ocular tissue fibrosis. *Endocr. Metab Immune. Disord. Drug Targets* **8,** 69–76
74. Immel, J., Negi, A., and Marmor, M. F. (1986) Acute changes in RPE apical morphology after retinal detachment in rabbit. A SEM study. *Invest. Ophthalmol. Vis. Sci.* **27,** 1770–1776
75. Zeng, R., Zhang, Y., Shi, F., and Kong, F. (2012) A novel experimental mouse model of retinal detachment: complete functional and histologic recovery of the retina. *Invest. Ophthalmol. Vis. Sci.* **53,** 1685–1695
76. Anderson, D. H., Stern, W. H., Fisher, S. K., Erickson, P. A., and Borgula, G. A. (1981) The onset of pigment epithelial proliferation after retinal detachment. *Invest. Ophthalmol. Vis. Sci.* **21,** 10–16
77. Lee, K. P., and Valentine, R. (1990) Retinotoxicity of 1,4,-bis(4-aminophenoxy)-2-phenylbenzene (2-phenyl-APB-144) in albino and pigmented rats. *Arch. Toxicol.* **64,** 135–142
78. Martín, F., Pastor, J. C., De La Rúa, E. R., Mayo-Iscar, A., García-Arumí, J., Martínez, V., Fernández, N., and Saornil, M. A. (2003) Proliferative vitreoretinopathy: cytologic findings in vitreous samples. *Ophthalmic Res.* **35,** 232–238
79. Casaroli-Marano, R. P., Pagan, R., and Vilaró, S. (1999) Epithelial-mesenchymal transition in proliferative vitreoretinopathy: intermediate filament protein expression in retinal pigment epithelial cells. *Invest. Ophthalmol. Vis. Sci.* **40,** 2062–2072